January 2014

Miniaturized Antenna Design For Wireless Biomedical Sensors

Mohannad M. Alharbi

MINIATURIZED ANTENNA DESIGN FOR WIRELESS BIOMEDICAL SENSORS

By

Mohannad Alharbi

Bachelor of Science, King Fahd University of Petroleum and Minerals, 2010

A Thesis
Submitted to the Graduate Faculty

of the

University of North Dakota

In partial fulfillment of the requirements

for the degree of

Master of Science

Grand Forks, North Dakota
August
2014

This thesis, submitted by Mohannad Alharbi in partial fulfillment of the requirements for the Degree of Master of Science from the University of North Dakota, has been read by the Faculty Advisory Committee under whom the work has been done, and is hereby approved.

Sima Noghanian_____
Chair person

Reza Fazel-Rezai_____

Arash Nejadpak_____

_____

_____

This thesis is being submitted by the appointed advisory committee as having met all of the requirements of the Graduate School at the University of North Dakota and is hereby approved.

Dr. Wayne E. Swisher_____
Dean of the Graduate School

_____
Date

Title Miniaturized Antenna Design for Wireless Biomedical Sensors

Department Electrical Engineering

Degree Master of Science

In presenting this thesis in partial fulfillment of the requirements for a graduate degree from the University of North Dakota, I agree that the library of this University shall make it freely available for inspection. I further agree that permission for extensive copying for scholarly purposes may be granted by the professor who supervised my thesis work or, in her absence, by the Chairperson of the department or the dean of the Graduate School. It is understood that any copying or publication or other use of this thesis or part thereof for financial gain shall not be allowed without my written permission. It is also understood that due recognition shall be given to me and to the University of North Dakota in any scholarly use which may be made of any material in my thesis.

Mohannad Alharbi
July, 28 2014

TABLE OF CONTENTS

LIST OF FIGURES

LIST OF TABLES

ACKNOWLEDGEMENTS

I wish to express my sincere appreciation to my advisor Professor Sima Noghanian, the members of my advisory committee Professors Reza Fazel-Rezai, and Arash Nejadpak for their guidance and support during my time in the master's program at the University of North Dakota. Also, I would like to thank Professor Isaac Chang, Professor Saleh Faruque and Lindsey Wiest, Mohamed Radwan, and Ivana Brzonova for their help. As well I would like to express my appreciation to Ministry of Higher Education of Saudi Arabia for the financial assistance in my research.

To: My Parents Mohammadsalih Alsati and Huda Almalki

ABSTRACT

This thesis is focused on the design and simulation of miniaturized antennas for wireless biomedical sensors. The motivation of the work was to provide a solution for wireless systems that are embedded or placed on the body. Currently, small antennas are on demand to be implanted inside the body or placed closely to the body. The performance of such antennas, gain and efficiency, is affected by the lossy tissues that surround them. The goal of this work was to design antennas that are placed on a living body and integrated with a sensor system implanted in living tissue, to measure the dielectric properties of the tissue. The antenna type that this work was based on is Planar Inverted F Antenna (PIFA). The assumption was that the antenna is placed on skin layer and not embedded inside a tissue layers. A few antennas were designed and simulated. Two major studies were performed. First, an antenna, which was originally proposed in literature for wireless communication systems, was adopted and revised for biomedical applications. The antenna performance while it was on two tissue layers (skin and fat) was studied and optimized. The objective was to understand how miniaturization and the surrounding environment affect the antenna resonance frequency and performance. A second study was performed to design a novel PIFA antenna to improve the performance and reduce the size further.

CHAPTER 1 INTRODUCTION

Microwave Imaging (MI) is a promising technique for detecting cancer in early stages [1]. MI technique compensates the drawback of other diagnostics techniques. MI method relies on the electric properties of the targeted tissue. One of the causes that prevent the use of this technique is the lack of accurate values of tissues' electrical properties measured *in vivo*. Despite the number of research activities in this field, there is no accurate database of such information. To overcome this issue, biocompatible dielectric sensors that can be implanted inside tissues should be developed. To provide the mobility during the measurements these sensors need to operate in a wireless setup. Therefore, small antennas are needed to be integrated with sensors and be mounted on the body (initially on small animal e.g. rats). This thesis focuses on designing small antennas within the size of 3.5 X 3.5 X 3.5 mm^3 and operating at frequencies below 10 GHz.

1.1 Motivation

Miniature antennas are of interest for usage in medical applications such as wearable or implanted systems for heat generation used in hyperthermia treatment [2][3]. In this thesis our focus, is biotelemetry applications.

Nowadays, the demand is for wearable wireless health monitoring and biomedical diagnostics systems. Antenna is one of the major limiting factors when it comes to miniaturizing these systems. The challenge is designing small, efficient antennas with good polarization purity and high gain at low frequency [4]-[6]. In addition, small

antennas are sensitive to the surrounding environment; especially when the antenna is placed close to dispersive and lossy materials such as biological tissues. Tissues are dispersive and lossy; they absorb power or dissipate it as heat, and they work as impedance load resulting in impedance mismatch from which the system losses become significant [2]-[7].

This thesis is a step toward the realm of small antennas. Most of the previous works on designing implanted antennas show that when the antenna is inside or closed to the tissue layers the gain degradation is evident [8]. Most of the antennas proposed in the literature are designed at low frequency band such as Medical Implanted Communications (MICS); and industrial, scientific, and medical (ISM). Hence, the size of the antenna are large and makes a load on the rats.

In this work, the miniaturized antenna was optimized in terms of the dimensions, shape and performance (gain and matching) to work at frequencies less than 10 GHz. It is shown that gain has values higher than -7dBi. The antenna was built and tested on phantom that possesses similar electrical characteristics to fatty and skin tissues.

1.2 Thesis Outline

1.2.1 Chapter 2: Literature Review

In this chapter, we introduce the role of microwave frequency in clinical imaging, and its relation with electrical properties of biological tissue. Hence, it provides a brief overview regarding fundamental antenna parameters, and the limitation of small antennas.

1.2.2 Chapter 3: Small Antennas Design

This chapter introduces the design of small antennas and their interactions with biological tissues. First design is based on an antenna that was proposed in literature for mobile communication applications. An antenna was proposed based on this design and the effects of tissue layers (skin and fat) on the antenna were considered. The antenna was optimized for better performance. The second antenna proposed in this chapter is a novel design acquired by performing parametric study.

1.2.3 Chapter 4: Study of Miniaturized Antenna on Head

Antenna was designed and optimized to be part of array of sensors close to the head. A comparison between custom head tissue and realistic head model were conducted to observe how the antenna performance change with a curvy shape and to what extent the performance influenced by tissues that have different dielectric properties from skin and fat.

1.2.4 Chapter 5: Optimization and Fabrications

Further antenna optimization and testing fabricated antenna were discussed in this chapter. The optimization was done for two reasons. The first reason is to ease the novel antenna fabrication. Another reason is to make it independent from the tissue layers. One of the proposed antennas was fabricated and tested in free space and on phantom and measured values were compared with the simulation results.

1.2.5 Chapter 6: Future Work and Conclusions

This chapter addresses further consideration regarding antenna design and fabrication. It highlights the issues that are associated with the antenna-sensor system design.

CHAPTER 2 LITERATURE REVIEW

2.1 Microwave Imaging and Dielectric Properties

Microwave frequencies have been used in many applications such as radar system, communication and heating [9]. Recently, much research has been conducted on medical imaging using microwave frequencies. MI is a promising technique in medical diagnostics [1]. One of the proposed applications of microwave imaging is breast cancer detection. Currently, mammography, ultrasound, and MRI are used for breast cancer screening. However, MI technique compensates some of the drawback of other diagnostics techniques. Unlike X-ray, MI is safe since it is non-ionizing. Also, as compared to MRI diagnostics, MI is more affordable.

MI works by transmitting microwave field to the target and measure the scattered fields. The scattered fields' strength depends on the contrast of dielectric properties of the tissues. Knowing the true value of dielectric properties is necessary for utilizing MI diagnostic techniques. Many papers have been published on measuring dielectric values of several tissues [10], [11] and [12]. Depending on the environment surrounding the tissue under test, these measurements are classified as *in-vivo*, *ex-vivo*, and *in-vitro*.

2.1.1 Dielectric Properties Concept

Microwave is a division of electromagnetic waves. Its frequency band ranges from 3 to 300 GHz. In a realm of the electric phenomenon, materials are classified into three types: conductors, semi-conductors and insulator. Dielectrics fall under insulator materials. An atom of dielectric has positive charge, nucleus, and cloud of negative charges, electrons. Since the positive charges equalize the negative ones, atoms are neutral. When the electric field is applied to the atoms, the positive charges are displaced in the direction of the electric field, and the electrons drift in the other direction. This will create an electric dipole. The multiplication of the distance between the positive and negative charges and the value of charge is called *dipole moment* and its direction is from negative to positive charge as seen in Figure 1.

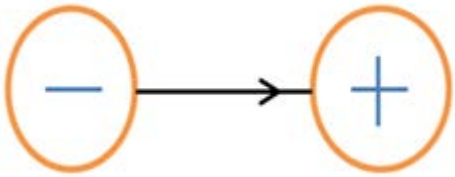

Figure 1. Dipole phenomena.

There are two types of dielectric materials: nonpolar and polar dielectric materials. Non-polar materials do not have dipoles such as hydrogen, oxygen, nitrogen, and the rare gases; dipoles are induced when the electric filed is applied to the materials. On the other hand, polar materials have dipoles without electric field application for example, water, sulfur dioxide, hydrochloric, and biological tissue. Due to application of the electric field, dipole moments align in the direction of electric field, and this

phenomenon is called *polarization* [9]. The time the dipole moments take to reach a saturated value is defined as relaxation time (τ) [13]. The process of polarization and electric field application is clarified in Figure 2.

From external filed angular frequency (ω) and relaxation time (τ), two properties characterize dielectric material upon electric field application. Those properties are permittivity (ε) and conductivity (σ).

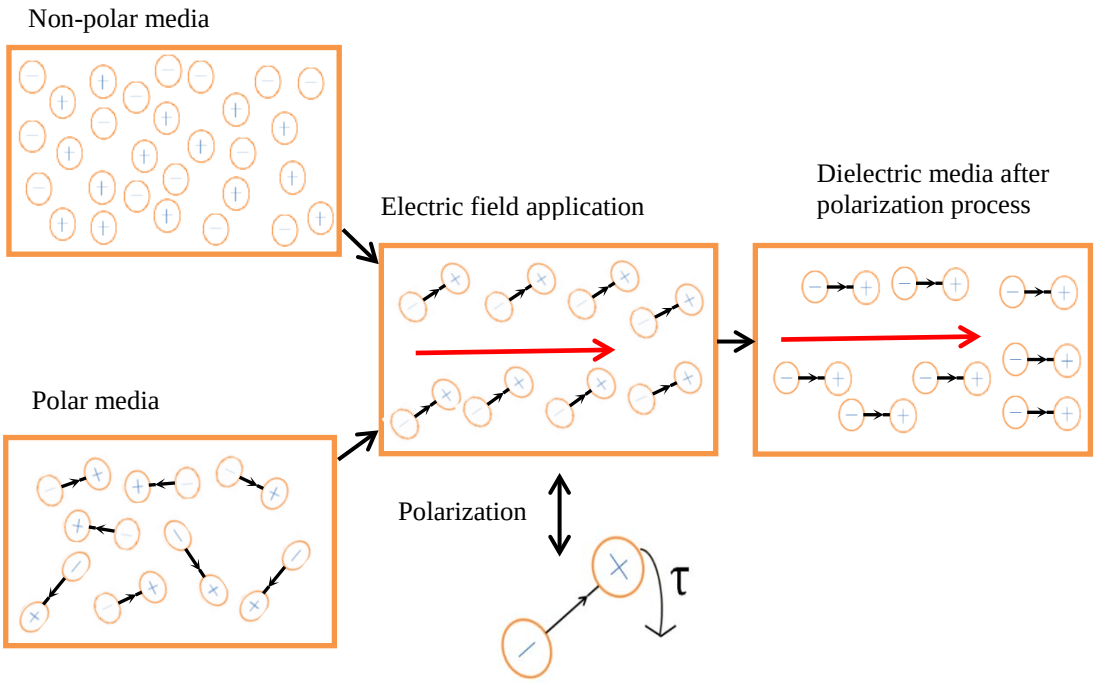

Figure 2. Polarization and electric field process.

Permittivity (ε) is parameter that reflects how many bound charges (not free to move) are displaced during polarizations. Conductivity (σ) describes how many free charges move in dielectric material upon applying electric field on that material [14]. The conductivity of the tissue at microwave range is ionic which is different from conventional conductivity resulted from free electrons.

2.1.2 Microwave Fields and Imaging Mechanism

Microwave fields can propagate inside different tissue. A part of the field is absorbed and the other part is scattered. The scattered fields are detected to build an image of the dielectric profile of the object. This process is depicted in Figure 3. In interaction between electromagnetic field and biological material, three parameters that characterize the dielectric properties of a biological tissue are permittivity (ε), conductivity (σ), and permeability (μ). Biological materials are assumed to be non-magnetic, and therefore, have permeability the same as free-space permeability (μ_o). Hence, the electrical properties of tissues (permittivity and conductivity) are of interest [15].

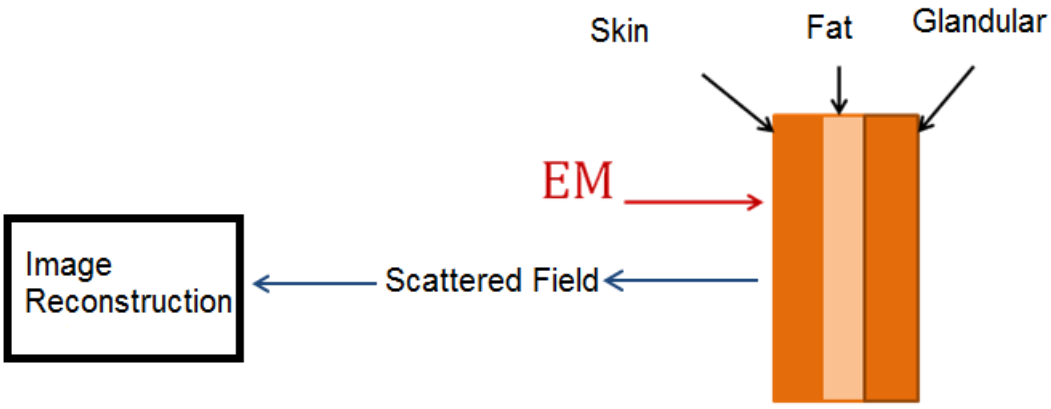

Figure 3. Interaction of EM field with biological material and image reconstruction.

Biological tissues are lossy and have high conductivity [8], [16]. For example, human breast is composed of several layers: skin, fat, and glandular tissues. Penetration depth (δ), which depends on the conductivity (σ) of the biological material and the frequency of the incident field (ω), is measured by the distance to which the microwave power penetrating the tissue decreases to $1/e$ of its value [17]. When the field is impinges

the breast, the skin converts a part of the incident flied to heat. Due to these losses the penetration depth is reduced in compare to free-space. Figure 4 depicts the penetration depth concept. Fatty tissue, that is the layer beneath skin, also reduces the penetration depth. As a result, the resolution of the acquired image is affected [16].

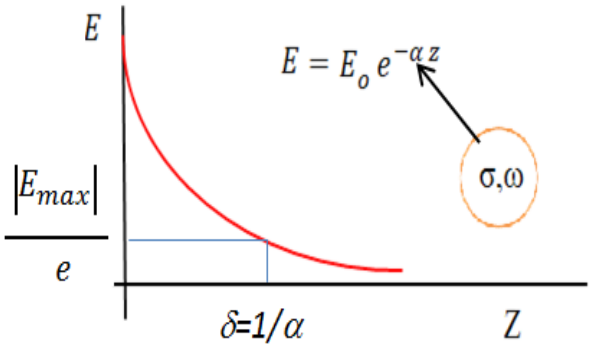

Figure 4. Penetration depth and electric strength in material.

It is desirable to have the highest image resolution possible. Resolution is dependent on the narrowest distance between two adjacent objects so that these two objects are distinguishable in an image. If the distance between two objects is shorter than the resolution of the image system, one object will be shown instead of two. The resolution is dependent upon the wavelength of the incident filed, which is inversely proportional to the frequency of external electric field as seen in equation (1).

$$\lambda = \frac{(v)2\pi}{\omega} \tag{1}$$

where (v) and (λ) are the velocity and the wavelength of the wave. The shorter the wavelength, which means higher frequency, the better resolution is obtained. However, the penetration of the field through the tissue decreases, as wavelength gets shorter. This

is because the conductivity of the biological material increases as the frequency of the external electric field increases [16].

2.1.3 Dielectric Properties Measurement

2.1.3.1 *Theoretical Measurement*

The permittivity is a complex number represented by equation (2).

$$\varepsilon^* = \varepsilon' - j\varepsilon'' \tag{2}$$

where ε' is the real part of the complex permittivity called dielectric constant, which evinces the energy stored and the dielectric material, and ε'' is the imaginary part which is known the dielectric loss expressing the energy absorption in the material. Energy absorption is caused by two phenomena, dielectric loss of dipoles rotation (ε_d''), and ionic conductivity (ε_σ'').

Energy loss associated with dielectric loss of dipoles rotation (ε_d'') is because some dipoles lag the external electric field [14]. Ionic conductivity contributes to the energy absorption in the biological material during external electric field submission. Energy absorption is performed by converting electric field to heat [17].

Dielectric loss of dipoles rotation (ε_d''), and ionic conductivity (ε_σ'') is described by equation (3) [17].

$$\varepsilon'' = \varepsilon_{\mathrm{d}}'' + \varepsilon_{\sigma}'' = \varepsilon_{\mathrm{d}}'' + \frac{\sigma}{\omega\varepsilon_{\mathrm{o}}} \tag{3}$$

where ω is the angular frequency of the external electric field, and ε_o is the free-space permittivity with the value of 8.854×10^{-12}F/m.

Dielectric constant and dielectric loss with single relaxation time are defined by Debye formulas (4-6) [14], [18].

$$\varepsilon' = \varepsilon_\infty + \frac{\varepsilon_s - \varepsilon_\infty}{1+\omega^2\tau^2} \tag{4}$$

$$\varepsilon'' = \frac{(\varepsilon_s - \varepsilon_\infty)\omega\tau}{1+\omega^2\tau^2} \tag{5}$$

$$\varepsilon^* = \varepsilon' - j\varepsilon'' = \varepsilon_\infty + \sum_n \frac{\varepsilon_s - \varepsilon_\infty}{1+(j\omega\tau_n)} - j\frac{\sigma_i}{\omega\varepsilon_o} \tag{6}$$

where ε_s and ε_∞ are the dielectric constant measured at low frequency and at high frequency.

Cole-Cole model characterizes the dielectric properties more accurately than Debye model. However, Debye model is used because of its less computational intensity. Cole-Cole equation is given in (7).

$$\varepsilon^* = \varepsilon' - j\varepsilon'' = \varepsilon_\infty + \sum_n \frac{\varepsilon_s - \varepsilon_\infty}{1+(j\omega\tau)^{1-\alpha_n}} - j\frac{\sigma_i}{\omega\varepsilon_o} \tag{7}$$

where α describes the distribution of the relaxation time [18]-[19].

2.1.3.2 *Practical Measurement*

2.1.3.2.1 Open-ended Coaxial Probe Method

Open-ended coaxial probe (OPC) measurement setup commonly consists of network analyzer, probe and software [20]. To measure the dielectric properties, the probe is in touch with the material, and the sensory part of the probe is stimulated with transverse electric and magnetic (TEM) field. The network analyzer measures the transmitted and reflected wave to get the reflection coefficient. Hence, the complex dielectric permittivity could be provided from the reflection coefficient. OPC is utilized to measure medium-loss and high-loss material. Advantages of OPC include availability

of commercial instrumentation, wide frequency range measuring, and nondestructive testing [17]. However, an error may be caused by air-gap between the probe and the material being tested, and accuracy of measurements may become low. Also, the material is presumed to be homogenous, isotropic, and non-magnetic. Furthermore, sample thickness has to be large enough to look infinite to the probe [20].

2.1.3.2.2 Transmission Line Method

Transmission Line Method (TLM) requires a network analyzer, coaxial cable or waveguide, and software. Permittivity and permeability are measured by reflection coefficient (S_{11}) and transmission coefficient (S_{21}). There are limitations regarding the material being tested. For coaxial cable and waveguide, the material has to be accurately inserted in cross section leaving no air gap. Furthermore, when the coaxial cable is utilized, the material inserted is made in toroid shape, which is difficult to make. Another limitation is that the material is assumed to be homogenous [20]. In spite of these disadvantages, TLM provides decent accuracy; unlike OPC, it can measure properties of magnetic and anisotropic media.

2.1.3.2.3 Resonant Cavity Method

Resonant Cavity Method (RCM) is used to evaluate the complex dielectric permittivity of lossy materials. A resonant cavity system is typically composed of a network analyzer, a cavity (rectangular and cylindrical), and a computer. The basic idea of this method is influencing the quality factor (Q) and the center frequency (f) of the cavity [20]. Perturbation Method (PM) is the most common resonant cavity method, which is based on comparing certain electrometric characteristics between empty and partly filled rectangular or cylindrical resonance cavity [17]. High accuracy is an

advantage of resonant cavity method. However, there are some limitations. Error in results emerges when the frequency resolution of the network analyzer is not high. In addition, dielectric measurements are provided at a single frequency, and a precise knowledge of physical shape of the sample is required [20].

2.1.3.2.4 Free Space Method

Free Space Method (FCM) is used to measure dielectric properties without a direct contact with the sample under test. The free space system comprises a vector network analyzer, instruments (antenna, arches, tunnel, etc.), software, and a computer (unless the programmable network analyzer is utilized). It is easy to measure the dielectric properties of the sample when it is heated at high temperature or put in hostile environment. Nevertheless, network analyzer calibration is a challenge. Table 1 lists a summary of the methods.

Table 1: Comparison of dielectric measurement methods.

Measurement Method	**Frequency**	**Accuracy**	**Dielectric Properties Measured**
Open-ended coaxial probe (OPC)	Wideband	Low	Electric only
Transmission line method (TLM)	Wideband	Medium	Both electric and magnetic
Resonant cavity method (RCM)	Single Freq.	High	Both electric and magnetic
Free space method (FSM)	Wideband	Low	Electric only

2.1.4 In-vitro, Ex-vivo, and In-vivo Measurements

Much research has been performed to provide the dielectric properties values of biological tissues *in-vitro*, *ex-vivo*, and *in-vivo*. *In-vivo* study is the process of measuring

or experimenting on a biological tissue in the living body whereas *ex-vivo* and *in-vitro* are studies on the tissue after it is excited from the body for simplicity and low cost. However, *ex-vivo* and *in-vitro* studies are different. *In-vitro* study is associated with tissue cells enclosed in a test tube. The purpose of the test tube is to keep the cells alive by providing an artificial environment so that long period test can be conducted. In *ex-vivo* studies, the measurement and experiment are done directly on a tissue as one unit that is directly removed and isolated from the body [21].

Several factors cause differences between *in-vitro, ex-vivo,* and *in-vivo* dielectric properties values and the methods of measurements might be very different for each case. Factors that influence dielectric properties are water content, temperature, and blood circulation.

It is claimed in [10] that the difference between *in-vivo* and *in-vitro* measurement is influenced by changes of blood content. In another research [22], it was found that the permittivity and conductivity of *in-vivo* are higher than that of *ex-vivo* at microwave frequencies because the drop in the dielectric properties of excised tissues are result of temperature variation, tissues desiccation, and blood circulation loss. Also, a study on liver tissues [12] at 915 MHz and 2.45 GHz reported that the *in-vivo* dielectric properties of normal and malignant liver tissues are not substantially different while noticeable divergence is exposed between *ex-vivo* normal and malignant liver tissues; this is because temperature and water content changes normally cause the divergences between *in-vivo* and *ex-vivo* dielectric characteristics of a tissue.

Different types of biological tissue possess different dielectric properties values. For instance, in [11] it was observed that fat tissue of the mice breast was distinguished from cancerous tissue; however, the difference between tumor and muscle was less distinguishable because muscle has higher water content than tumor has. Likewise, study of [10] reported that the inner organs, which are liver, kidney, spleen, and gray matter of the brain exhibit electromagnetically heterogeneous behavior. The heterogeneity of a tissue is likely a result of a change in blood circulation and content of water. Furthermore, it is possible that the difference between smooth and skeletal muscles permittivity at a frequency higher than 100MHz is a result of water content or concentration of ions. Table 2 presents some of prior work on measuring dielectric properties.

Table 2: Prior work on measuring dielectric properties.

Ref. #	**Publication Date**	***ex-vivo/ in-vivo/in-vitro***	**Tissue Samples**	**Measurement Methods**	**Frequency Range**
[10]	1981	*in-vivo*	Feline tissues (Skeletal and smooth muscles, liver, kidney, spleen, and gray and white matters of brain).	Open-ended coaxial line sensor	10 MHz – 1 GHz
[23]	1982	*in-vivo* and *in-vitro*	Cat tissues (Muscles, spleen, kidney cortex, liver, and brain cortex.)	Open-ended coaxial cable	100 MHz – 8 GHz
[24]	1991	*in-vitro*	Human breast tissue	Resonant cavity method	3.2 GHz
[25]	1991	*in-vitro*	Abdominal of mice	Capacitive sensor	10 kHz – 100 MHz 10 kHz – 2 GHz
[11]	2006	*in-vivo*	Mice breast tissue	Conventional probe Novel probe	0.5 GHz - 30 GHz
[12]	2007	*ex-vivo* and *in-vivo*	Human liver tissue	Open-ended coaxial cable	0.5 GHz - 20 GHz
[22]	2009	*ex-vivo* and *in-vivo*	Human breast tissue	Electrical impedance spectroscopy probes (EIS) Microwave impedance spectroscopy probe (MIS)	100 Hz- 1 MHz (ex-vivo EIS) 100 Hz – 100 KHz (in-vivo EIS) 0.1 GHz – 8.5 GHz (ex-vivo MIS)
[26]	2012	*ex-vivo*	Mice breast tissues	Open-ended coaxial probe Two-port sample holder	50 MHz – 5 GHz

2.1.5 Summary of Dielectric Property

This section introduced the role of microwave frequency in clinical imaging, which is based on the contrast of dielectric properties of different tissue types. The interaction of electrical field with biological media, the electrical properties involved in this process, and the resultant influence on the resolution of an image were reviewed. The theoretical and various practical measurements of dialectic properties were presented. It was discussed how dielectric characteristics values in *in-vivo*, *ex-vivo*, and *in-vitro* are affected by some factors in the tissues.

2.2 Antenna Concepts

Antenna is an important part of wireless communication. It is an element that transforms signals or voltages in wires to electromagnetic waves to be transmitted, and it does the reversal process; which is receiving electromagnetic waves and transforming it to signals or voltage [27]. There are different types of antenna such as dipole, helix, loop, microstrip patch, lens, and reflector antennas. More information on these types is provided in [28]. A brief overview regarding the parameters of antenna is presented here.

2.2.1 Essential Antenna Parameters

2.2.1.1 *Radiation Pattern*

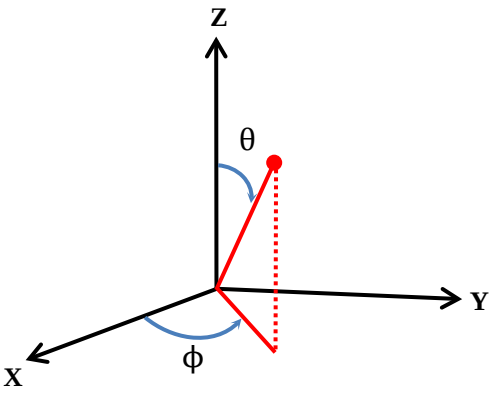

Figure 5. Spherical coordinates.

A configuration of radiated energy that is presented by a function of directional coordinates (for practical applications, spherical coordinates are utilized, as seen in Figure 5). There are three types of patterns. One type of patterns is isotropic. Isotropic pattern is produced by a hypothetical lossless infinitesimal antenna (point source) that radiates uniformly in all directions. Though it is non-existing pattern, it is used as reference for directivity concept of actual antennas. Another pattern is omnidirectional pattern that is not directional in a given plane and directional in the orthogonal plane [28]. The third type is the directional pattern that is directed towards a specific angle.

2.2.1.2 *Directivity and Gain*

Electromagnetic waves are the means for caring information wirelessly. Power and energy are elements for evaluating electromagnetic field quantity. Hence, the radiated power (averaged power) of the antenna is calculated by (8).

$$P_{rad} = P_{ave} = \oiint_S \boldsymbol{W_{rad}} \cdot d\boldsymbol{s} = \frac{1}{2} \oiint_S Re(\boldsymbol{E} \times H^*) \cdot d\boldsymbol{s} \quad (8)$$

where P_{rad} and P_{ave} are the radiated power and average power, respectively, W_{rad} is the radiated power density. $\boldsymbol{E}$ and $\boldsymbol{H^*}$ are the complex electric field and the conjugate magnetic field.

Radiation intensity is another parameter associated with electromagnetic field. It is related to the radiated power density and total radiated power as depicted in (9) and (10)

$$\mathrm{U} = \mathrm{r}^2 \mathrm{W}_{\mathrm{rad}} \quad (9)$$

$$\mathrm{P}_{\mathrm{rad}} = \int_0^{2\pi} \int_0^{\pi} \mathrm{U} \sin\theta \, \mathrm{d}\theta \, \mathrm{d}\emptyset \quad (10)$$

Directivity (D) is an important parameter in antenna applications. It shows the directionality of radiation intensity of the antenna in compare to an isotropic source. Its value is than greater or equal to 1 (0 dB), it is unit less and it is evaluated by (11).

$$D = \frac{4\pi U}{P_{rad}} \quad (11)$$

Gain (G) is the parameter, which governs the performance of the antenna. The gain is related to the directivity by the antenna radiation efficiency, or conduction-dielectric efficiency (η_r) and impedance mismatch, measured by reflection coefficient (Γ). Antenna radiation efficiency depends on two parameters: radiation resistance of the antenna (R_r) and conduction-dielectric losses, which is represented by resistance (R_L). The gain and radiation efficiency are shown in (12) and (13) [28].

$$G = D \, \eta_r \, (1 - \Gamma) \quad (12)$$

$$\eta_r = \frac{R_r}{R_r + R_L} \quad (13)$$

2.2.1.3 *Bandwidth*

Antenna bandwidth is (B) is the band of frequency where the antenna has an efficient performance. Bandwidth can be expressed in two ways. If the antenna is broadband, the bandwidth is evinced as (upper frequency: lower frequency). For example, if the upper frequency is 15 times greater than the lower one, the bandwidth is 15:1. Another expression is for narrow band antennas as given in (14).

$$B(\%) = \frac{f_h - f_l}{f_c} \times 100 \tag{14}$$

where f_h , f_l,and f_c are the upper , lower , and the center frequencies, respectively[28].

2.2.1.4 *Polarization*

Polarization is the parameter that defines the direction of electric field with varying time and the relative magnitude of the electric field. Polarization is divided in to 3 types: linear polarization, circular polarization, and elliptical polarization. In linear polarization, the electric field magnitude is changing on one axis. In elliptical and circular polarization, the magnitude of the electric field is changing on a 2-D plane in circular or elliptical form. The types of polarizations are shown in Figure 6.

Linear and circular polarizations are special cases of elliptical polarization. The formula for instantaneous electric field $e(z,t)$ and the phase difference are presented in (15) and (16), respectively.

$$e(z,t) = \hat{a}_x\, E_{xo}\ cos(\omega t + kz + \emptyset_x) + \hat{a}_y\, E_{yo}\ cos\left(\omega t + kz + \emptyset_y\right) \tag{15}$$

$$\Delta\emptyset = \emptyset_y - \emptyset_x \tag{16}$$

where E_{xo} and E_{yo} are the maximum magnitudes, K wave number, ω is the angular frequency, and $\emptyset$ is the phase. The linear polarization is only obtained when the phase difference is a multiple of π. For a wave having circular polarization, the maximum magnitudes (E_{xo}, E_{yo}) must be equal and the phase difference equals to $n\frac{\pi}{2}$, where n is an odd integer. Elliptical polarization can be achieved by either a difference between the magnitudes of two components and the phase difference is odd multiple of $\frac{\pi}{2}$, or the phase difference is not multiples of $\frac{\pi}{2}$, (even if the equal magnitude condition exists).

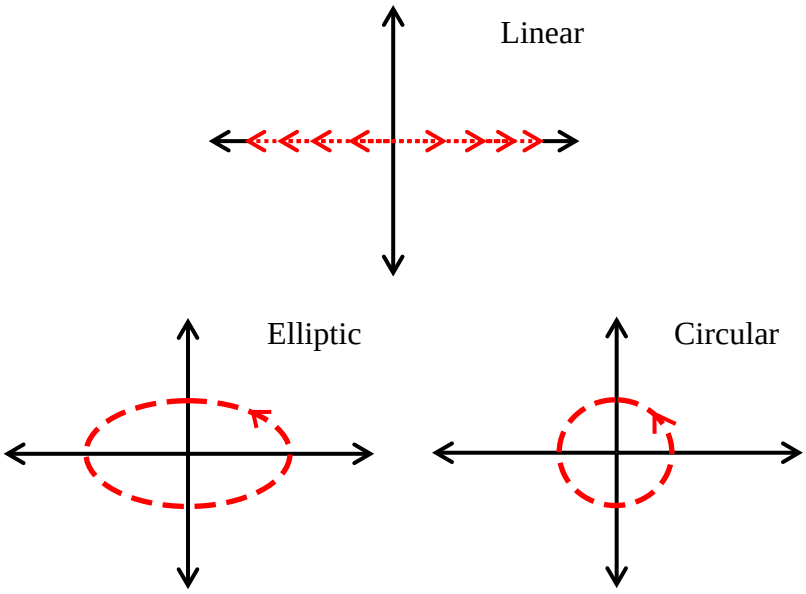

Figure 6. Polarization types.

Antenna's far-field is composed of two orthogonal components: co-polarization (co-pol) and cross-polarization (x-pol). Co-polarization is the intended polarization whereas cross polarization is orthogonal to the former, and it is usually undesirable since the receiving antenna will not receive this part of the signal. A depiction of the two components is shown in Figure 7. For example, assume that dipole antenna shown in this

figure is the receiver antenna. Dipole is linearly polarized, the co-polarized component of the received wave is the green line, and cross-polarization component is the red line.

In real application, the polarization of a receiving antenna will not be exactly the same as the polarization of the incoming wave. This case is known as polarization mismatch, and it is evaluated by polarization loss factor (PLF), which is stated in (17).

$$PLF = |cos\,\varphi|^2 \tag{17}$$

where φ is the angle between the polarization of the incident wave and the polarization of the receiving antenna. PLF unity means the polarization of the incent wave is the same as polarization of the receiving antenna, and the antenna obtains the maximum power from the incident wave. PLF equaling to zero refers to polarization mismatch, which results in no power reception [28].

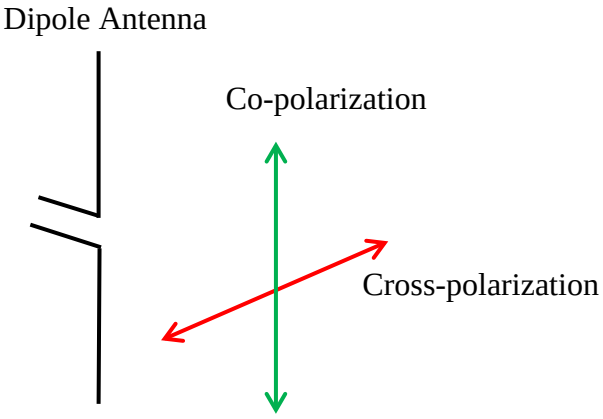

Figure 7. Co-pol and cross-pol description.

2.2.1.5 *Electrical Length*

Electrical length is different from physical length. Electrical length is a property that expresses the length of a transmission medium or antenna in terms of the signal

wavelengths (λ) that transmit through the medium. In free space, the velocity of electromagnetic field is assumed to be the velocity of light. In dielectric media, however, the velocity of wave in the medium is smaller. Therefore, the wavelength is smaller. Electrical length is the length in the units of wavelength. For example, if the wavelength in dielectric media is one half of the free-space wavelength at a certain frequency, the electric length in the media becomes twice larger than the free-space electrical length at the same frequency. This example is shown in Figure 8.

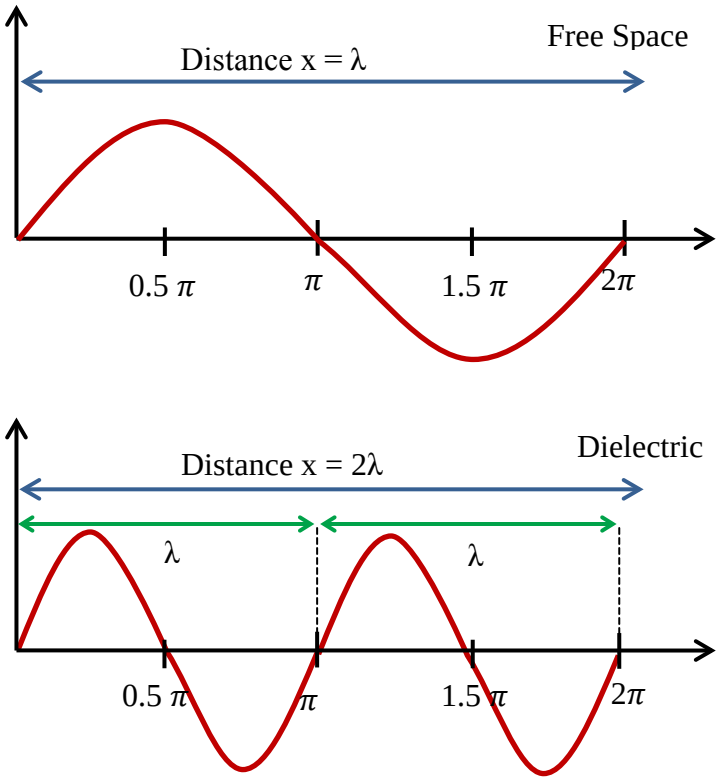

Figure 8. Explanation of electrical length in different media.

2.2.1.6 *Effective Area*

Effective area (A_e) is a parameter that describes the percentage of physical area that captures power in the receiving mode [28], and it is evaluated by (18).

$$A_e = \frac{P_T}{W_i} \tag{18}$$

where P_T is the power supplied to the load, and W_i is the power density of input wave [28].

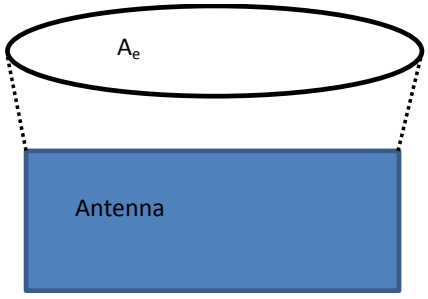

Figure 9. Effective area description.

2.3 Limitations of Antenna Miniaturization

Small wireless portable devices are used in many areas in our daily life. For example, wireless router for Internet connection, cell phones, wireless flash memories, wireless sensors, etc. Small antennas are deployed to send and receive data. Currently there is an emerging need for smaller devices, which leads to the need for smaller antennas; however, there are some limitations in reducing the size of the antenna because miniaturizing an antenna results in degradation in its performance such as lowering the gain, bandwidth reduction, and increasing the cross polarization level. The purpose of this section is to introduce small antennas' design limitations, and some methods to overcome or minimize their effects.

2.3.1 Background

Small antenna definition is not explicit. There are three different types of small antennas: electrically small antenna, physically small antenna, and functionally small antenna [29].

It is obvious that physically small antenna means the size of antenna is small; nonetheless, electrically and functionally small antennas do not necessarily include the physical meaning. Electrically small antenna is the one whose maximum dimension is surrounded by a sphere of radius $\frac{\lambda}{2}$ (Figure 10). At 900 MHz, for instance, antenna dimension is 0.33m (33.3 cm,) which is physically large compared to current portable devices and not convenient for usage in small-sized wireless applications. Functionally small antenna may not include electrical and physical definition; its dimension can be reduced by adding some functions to it, function that are not achievable by antenna having the same size [5], [29].

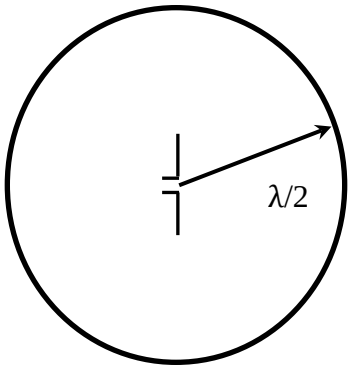

Figure 10. Imaginary sphere for electrically small antenna.

2.3.2 Effects of Miniaturizing Antenna on Performance

Reducing the antenna size affects its performance properties, which are impedance, efficiency, gain, effective area, and bandwidth.

2.3.2.1 *Impedance Mismatch*

Impedance mismatch between the antenna and the transmission line is one of the major problems. Impedance matching is tuning antenna's reactance to zero and transforming antenna's low resistance to 50 Ω or desired matching impedance [29]. As the antenna size is minimized, the reactance of the input impedance decreases, the antenna becomes capacitive, and does not radiate properly at resonance frequency [29]-[30].

Impedance matching may be achieved by one of these methods: changes within the antenna structure or adding external reactive components [30].

2.3.2.2 *Efficiency*

Degradation in the efficiency is another issue. Since miniaturizing the antenna makes it more capacitive, the energy is stored. As a result, there is little current flowing in the antenna, which produces low power. A simple illustration is depicted in Figure 11 [30]. Radiation efficiency can be enhanced by considering antenna configuration, dielectric losses, and choice of conductor diameter and thickness [30].

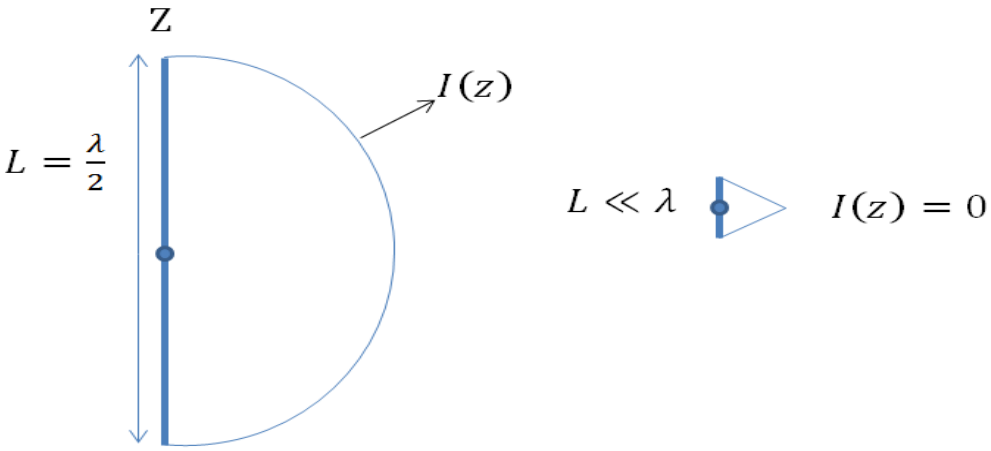

Figure 11. Current and size of antenna.

2.3.2.3 *Directivity and Gain*

The directivity and the gain (realized gain) of the antenna are also affected by the size of the antenna and the dielectric material, when it is included in antenna structure or surrounding. The antenna directivity depends on the antenna's electrical dimensions. The gain is always less than or equal the directivity. However, in small antenna, the directivity ranges from 1.76 to 2 dBi and does not change by the size of the antenna, and the gain becomes extremely smaller than the directivity [30]. Also, dielectric material inclusion for miniaturization purposes, for example substrate in planar inverted F antenna, has an influence on the gain. It is reported that dielectric material with high loss tangent reduces the gain [31].

The realized gain is practically limited by four factors [30]:

- Impedance matching between the antenna and transmitter, and minimization of losses within any matching network.
- High radiation efficiency depending on suitable choice of conductor diameter or thickness and dielectric losses mitigation.
- Reducing the effect of detuning.
- Minimizing polarization mismatch.

2.3.2.4 *Effective Area*

Miniaturization influences the effective area (A_e) of the antenna. In large antennas, effective area which is governed by the antenna dimensions is equal or less than the physical area. On the other hand, the physical area of the small antenna is smaller than the effective area, and effective area depends on the wavelength instead of the physical length. Figure 12 shows the relation between effective area and antenna size [30]. Please note that in this statement the physical area is only considered to be the antenna aperture physical area. In small antennas, the transmission lines and the ground plane also become important parts of radiation. Therefore, in reality the physical area might be larger than the effective area. But these are not included in the calculation of effective area.

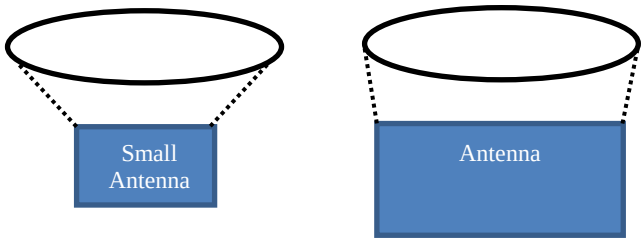

Figure 12. The relation between effective area and antenna size.

2.3.2.5 *Bandwidth*

Reducing the size of the antenna plays an important role in the bandwidth. Bandwidth has reciprocal relation with the quality factor. The quality factor is the ratio of the average energy stored in the circuit to the average power. As the quality factor increases the bandwidth decrease and vice versa. The quality factor formulas are presented by (19) and (20) [32].

$$Q = \frac{2\,\omega\, max\,(W_E, W_M)}{P_A} \tag{19}$$

$$Q \approx \frac{1}{B} \tag{20}$$

where Q is the quality factor, ω is the angular frequency, W_E is the stored electric energy, W_M is the stored magnetic energy, P_A is antenna received power, and B is the bandwidth.

As the antenna sizes decreases the quality factor increases, which means more reactive energy is stored. Consequently, the antenna acts like a capacitor [30].

Antenna bandwidth can be improved by various techniques. Using integration technique, which is loading one or more reactance components in the antenna makes variation in the current distribution on the antenna [5]. This leads to bandwidth

enhancement. In addition, including losses in the antenna could decrease the quality factor, and in turn, increase the bandwidth; however, this causes the gain reduction [28].

2.3.3 Summary

Small antennas are an important part in small wireless devices. However, designing small antenna with specific properties is not an easy task since miniaturizing antenna affects some characteristics such as gain, bandwidth and efficiency. In this section the limitations of antenna miniaturization and some methods to improve their performance were reviewed.

CHAPTER 3 MINIATURIZED ANTENNA DESIGN

3.1 Introduction

Small antennas are needed for current and future biotelemetry applications. The features required for such applications are: small physical size, low profile, being cost effective and easily manufactured. In this thesis we are focusing on design of electrically small antennas working at frequencies less than 10 GHz. Planar inverted F antenna (PIFA), as shown in Figure 13, is an attractive choice since it is consistent with these features. In addition, PIFA has low back lobe radiation, which reduces the radiation on the body and results in low specific absorption rate (SAR). However, narrow bandwidth is disadvantage of PIFA. Designing miniaturized antennas involves many challenges; one of these challenges is the surrounding environment effect on the antenna performance. Small antenna is sensitive to the surrounding environment; especially when the antenna is working closer to dispersive materials like biological tissues. Dispersive tissues are lossy; they absorb power or dissipate it as heat, which in turns causes degradation of efficiency. Additionally they work as impedance load resulting in impedance mismatch from which the system losses become significant [2], [7].

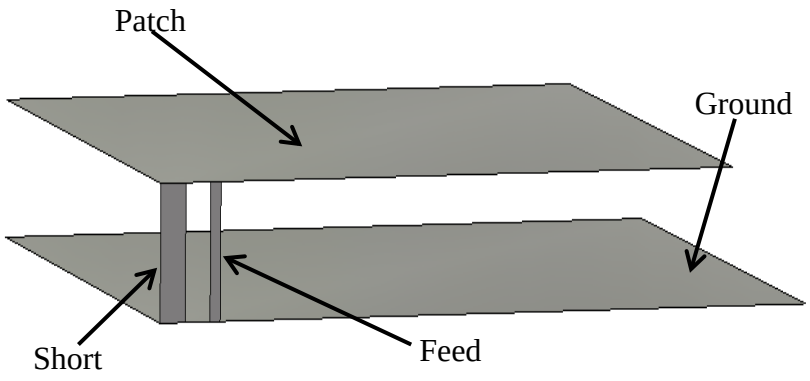

Figure 13. Common planer inverted antenna (PIFA).

For this thesis, the main goal was to design a small antenna for biotelemetry. Several antennas were investigated and modeled. In this chapter, two major studies for miniature antennas were performed. . The first study which is entitled miniaturized PIFA was based on a small antenna design which was proposed for mobile communication applications. Antenna size was adjusted and modified so that the effects of the surrounding (skin and fat tissues) were exploited. A second study is regarding a novel design that was acquired with parametric study while the antenna was placed on the tissue layers.

3.2 Miniaturized PIFA

3.2.1 Introduction

In this section we present a small PIFA design that has been optimized for the desired application in terms of limited volume and performance while placed on skin and fat tissues. All the simulations and optimizations are performed using commercial electromagnetic simulation software CST Microwave Studio [33]. Different optimization choices are also examined in terms of their run time. The three methods of interest were:

Trust Region Framework, Nelder Mead Simplex Algorithm, and Interpolated Quasi Newton. The objective was to design an antenna within the maximum volume of $18mm^3$, and resonating at a frequency less than 8GHz. The penetration depth is greatly reduced after this frequency. Therefore, most of microwave imaging systems work up to this frequency [34]. The antenna was first designed to confine with the required dimensions; then its performance was simulated and observed in free-space. Initially, the antenna was working at much higher frequency than desired. Therefore, several optimization steps were performed to reduce the resonance frequency while the dimensions were kept under the maximum size. After a reasonable performance was achieved in free-space, the antenna performance was studied and optimized when it was placed on lossy biological tissues including skin and fat layers.

3.2.2 PIFA Antenna Design and Optimization

3.2.2.1 *Antenna Design and Performance*

The design presented in [35] was selected as our starting point. The size was modified and the dimensions were chosen to confine with $18mm^3$ limitation. The antenna was simulated in CST Microwave Studio. Using high dielectric substrate helps reducing the size, however, the gain is degraded by the use of high permittivity substrates [31]. Therefore, Roger RT 5880 (ε_r=2.2, tanδ=0.0009) was chosen for substrate [36]. The antenna geometry is depicted in Figure 14, and its dimensions are listed in Table 3.

The antenna has two resonance frequencies as shown in Figure 15(a). The first resonance is at 8.88GHz, and the second one is at 14.90GHz. We aimed for S_{11} better than -10dB at the desired frequency, therefore, the lower resonance had to be matched to

provide the desired S_{11}. The frequency 8.88GHz is still relatively high to be considered as our lower resonance frequency.

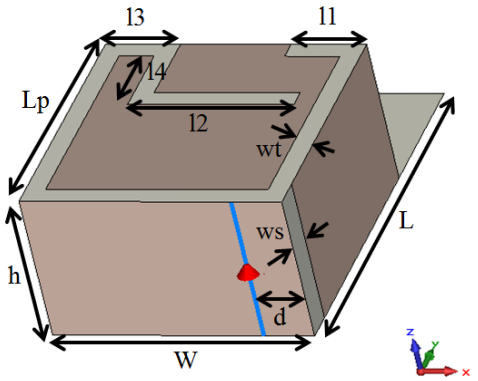

Figure 14. First PIFA design, simulated by CST Microwave Studio.

Table 3: First antenna dimensions.

Parameters	Value (mm)	Parameters	Value (mm)
Width (W)	2.6	Strips width (wt)	0.20
Length (L)	4.0	Strip 1 length (l1)	0.75
Patch length (Lp)	2.6	Strip 2 length (l2)	1.65
Feed position (d)	0.5	Strip 3 length (l3)	0.75
Substrate thickness (h)	1.5	Strip 4 length (l4)	0.80
Short width (ws)	0.3		

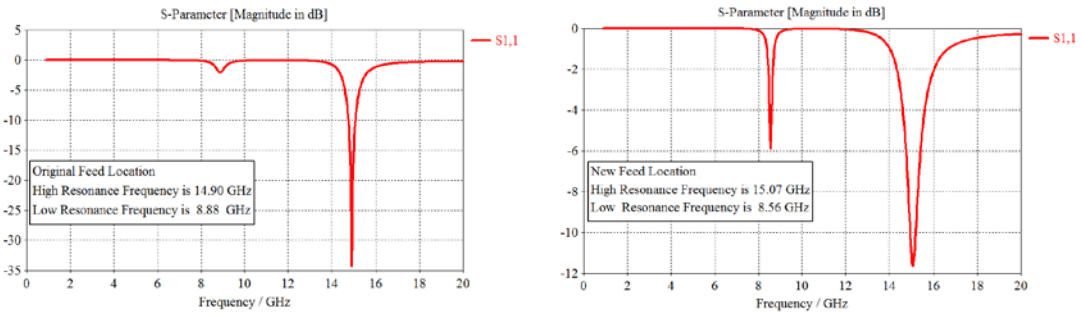

(a) (b)

Figure 15. Reflection coefficient of the first PIFA: (a) for original location of the feed, (b) after moving the feed.

Figure 16(a) shows the surface current density on the patch at 8.88GHz. The current does not pass through the short to the ground. This is because the feed has high impedance and blocks the current. To improve this, we changed the feed position and placed it on the same side as the shorting strip. Figure 15(b) shows the reflection coefficient of antenna after re-locating the feed. Figure 16(b) shows the current path after feed re-location. As expected, the current goes through the shorting strip to the ground which results in a change in the lower resonance frequency, moving it to 8.56GHz with S_{11} around -6dB, which is still higher than the goal (-10dB).

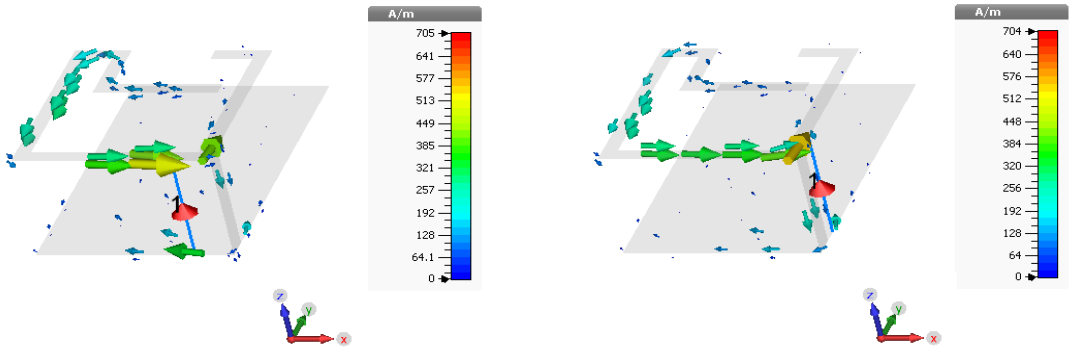

(a) (b)

Figure 16. Current densities on the patch at (a) 8.88GHz with the orinigal feed location, (b) 8.56 GHz after relocating the feed.

3.2.2.2 *Optimization*

Various parametric sweeps were done to discover which parameters have influence on return loss at the lower frequencies. It was found that substrate thickness (h), strip lengths l1 and l2, and feed position (d) (as shown in Figure 14) are the critical parameters. Nelder Mead Simplex Algorithm, Interpolated Quasi Newton, and Trust Region Framework are the optimization techniques provided by CST Microwave Studio.

These were utilized and their results were compared in terms of run-time and number of evaluations. Table 4 and Figure 17 present the number of evaluations and result of three optimization methods, respectively. All the three methods were able to move the higher resonance frequency, but were not very successful in moving the lower resonance frequency. Trust Region Framework and Nelder Mead Simplex Algorithm reduced S_{11} at low frequency to below -10dB.

Table 4: Comparison of three optimization methods.

Optimization Technique	**# of Evaluations**	**S_{11} (dB)**	**Resonance Frequency (GHz)**	**Gain (dBi)**	**Directivity (dBi)**
Trust Region Framework	8	-12.82	10.1340	0.64	1.42
Interpolated Quasi Newton	546	-6.66	9.8987	-0.34	1.31
Nelder Mead Simplex	181	-13.94	10.4970	0.49	1.38

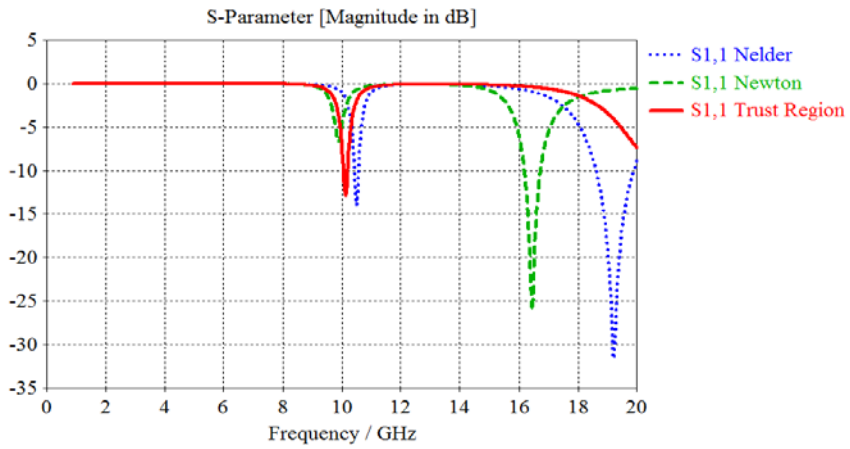

Figure 17. Reflection coefficient for optimized antennas: Trust Region method (solid red line), Interpolated Quasi Newton method (dashed green line), and Nelder Mead Simplex Algorithm (dotted blue line).

3.2.3 Performance of Antenna on Biological Tissue

3.2.3.1 *Initial Design and Performance*

The antenna optimized by the Trust Region Framework was placed on 1.5mm thick skin and 3.5mm thick fat, as shown in Figure 18. Tissues' dielectric properties were modeled by the first order Debye model. Table 5 provides the Debye parameters. The impact of tissue layers on the antenna's S_{11} is shown in Figure 19(a).

Table 5: Debye model parameters [37].

Tissue	ε_s	ε_∞	τ	**Area of Tissue**	**Thickness**
Skin	40.6	23.6	1.7×10^{-11}	$5 \times 5mm^2$	1.5mm
Fat	5.5	3.4	1.5×10^{-11}	$5 \times 5mm^2$	3.5mm

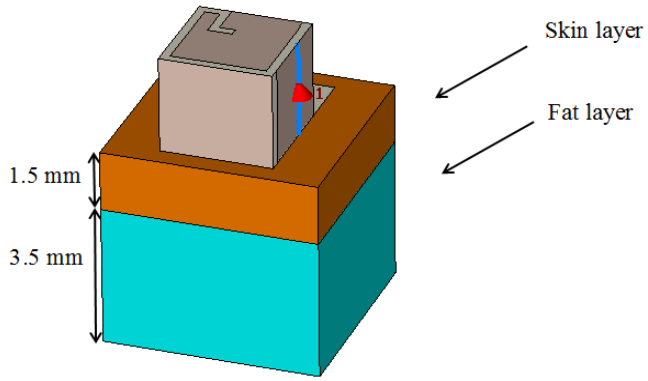

Figure 18. First PIFA design optimized by the Trust Region Framework is placed above the skin and fat layers.

3.2.3.2 *Antenna Optimization*

Since the Trust Region Framework method achieves the goal with less number of evaluations, it was used to decrease the return loss of the antenna and shift the resonance frequency to lower values after placing the tissue layers. Figure 19(b) shows the result of optimization. The resonance frequency was moved from 9.16GHz to 8.46GHz at the price of reducing the directivity from 3.05dBi to 2.86dBi. The antenna size was still larger than 18mm^3. Size reduction was achieved by reducing the ground plane length from 4.0mm to 2.6mm (the same as the patch length). As a result, the frequency shifted from 8.46GHz to 8.55GHz and the directivity was decreased to 2.21dBi (Figure 20).

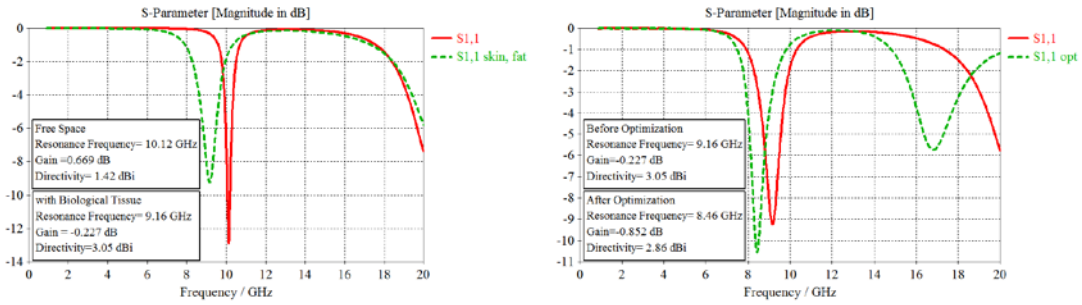

Figure 19. (a) Reflection coefficient in free-space (solid red line) and after placing on skin and fat layers (dashed green line), (b) reflection coefficient of the antenna before optimization (solid red line) and after optimization (dashed green line).

Further reduction of the resonance frequency is possible by adding slot on the ground to increase the current path on the ground [38]. Initially arbitrary dimensions were chosen for the slot in three major areas on the ground, one at a time, and it was concluded that the slot between the feed and the short (area 1) has significant effects on the resonance frequency and bandwidths (Figure 21). Consequently, the Trust Region Framework was utilized to optimize the slot size. The optimized antenna works at 6.55GHz (Figure 22, Table 6).

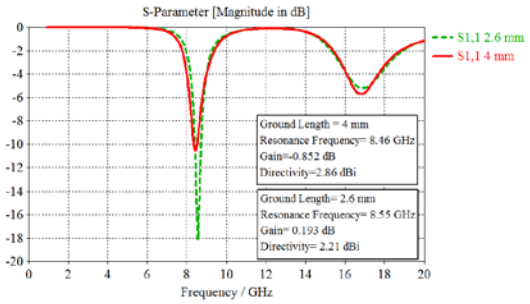

Figure 20. Reflection coefficient with ground plane length 4mm (solid red line) and 2.6mm (dashed green line).

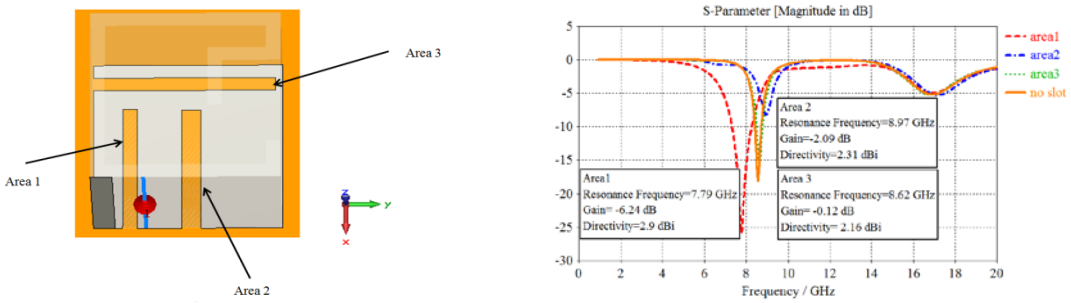

(a) (b)

Figure 21. (a) Different possible areas for placing the slot, (b) reflection coefficient for slot located in: area 1 (dashed red line), area 2 (dashed-dotted blue line), and area 3 (dotted yellow line).

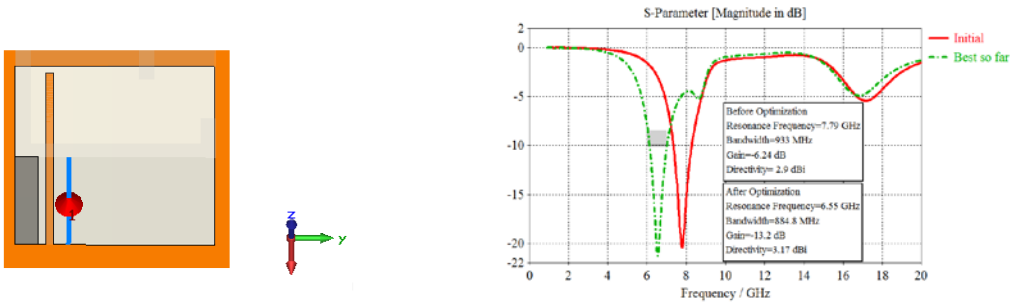

(a) (b)

Figure 22. (a) Optimized slot, (b) reflection coefficient before optimizing (solid red line), and after (dash dotted line).

Table 6: Original and optimized parameters in mm.

Parameters	Original Value	Range	Optimized Value
d	0.50	0.50-2.50	0.725
l1	0.75	0.00-1.65	0.569
l2	1.65	0.00-1.65	0.714
h	1.50	1.50-2.50	2.449

The antenna resonates at low frequency with good bandwidth. However, there are some issues. Figure 23 depicts the radiation pattern of the antenna. The cross-polarization level in the radiation patterns in the three cases is noticeable. Considering the broadside pattern (on z axis), the H field, which is the green dashed line (gain phi) on x-z plane, is the co-polarization field, and the cross-pol is shown as red line (gain theta). On y-z plane we have E-field. The co-polarization is shown as gain theta in red line. Also, the direction of the radiation is not desirable. The direction of the radiation pattern is not up-ward; it is partly directed toward the tissue.

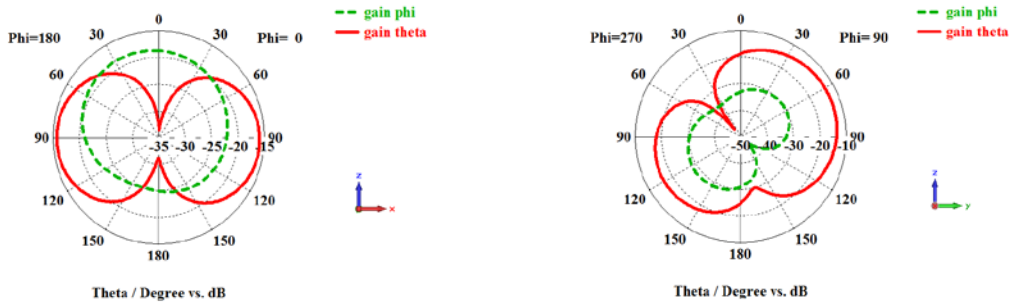

Figure 23. Radiation patterns of antenna along x-axis (H-plane) and y-axis (E-plane).

3.3 Novel Antenna Design

3.3.1 Introduction

In this design, two constraints were taken under consideration. First constraint is that the antenna is sensitive to the dispersive tissue layers; the performance degrades because of the high dielectric losses of the skin. Another constraint is the antenna with tissue layers becomes a complicated system; the resonance frequency and the radiation pattern are not predictable. Frist, a PIFA was designed above two tissue layers (skin and fat). Then a parametric study on the antenna was performed and the antenna parameters were optimized.

3.3.2 Antenna Structures

A conventional PIFA antenna was designed and was placed on tissue layers for simulation, as seen in Figure 24. The size of the antenna was within $20mm^3$. The size and dielectric parameters of tissues are similar to the ones in Section 3.2. The parameters for study are the slots' shape, its dimensions and position the patch. Also, slots' positions on the ground, substrates properties, and location of the shorting pin. Transition in parameters was governed by obtaining lower resonance frequency, reasonable reflection coefficient, broadside radiation pattern, and high co-polarization level. As a result, four configurations were suggested after a parametric study (shown in Figure 25).

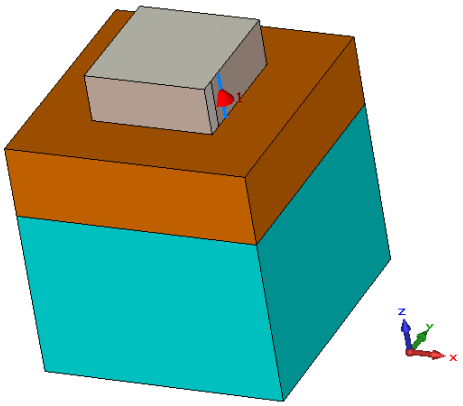

Figure 24. Conventional PIFA on skin (brown color) and fat (blue color).

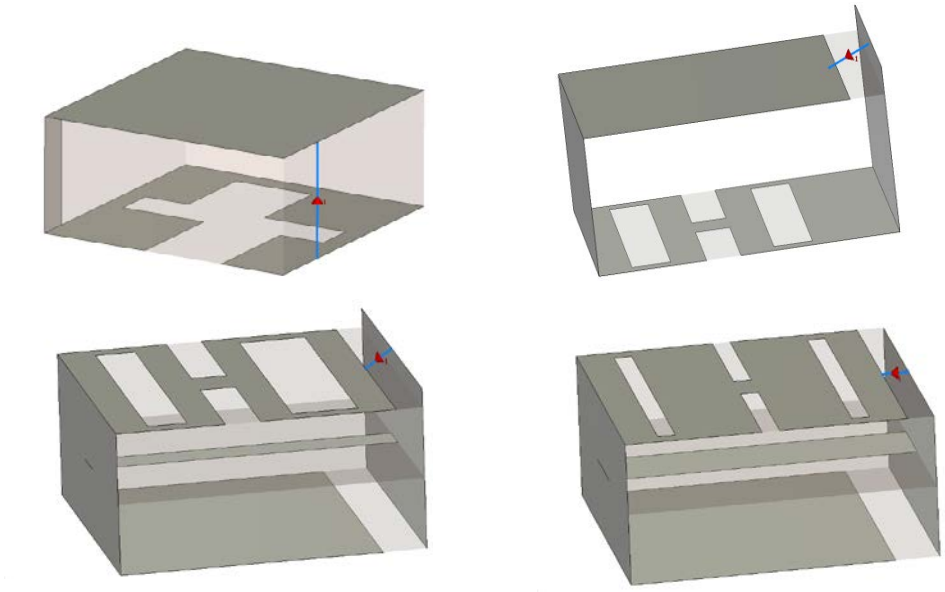

Figure 25. Four slot loaded PIFA desings.

3.3.3 Design Details

3.3.3.1 *Design 1*

The optimized antenna is shown Figure 26. The parameters of the antenna are listed in Table 7. The chosen substrate between the patch and the ground is Roger Ro 5880 with ε_r=2.2, and tanδ =0.0009. At the beginning, a conventional PIFA was designed using an Alumina 99.5% substrate (ε_r=9.9, tanδ =0.0001) since it is known that dielectric substrate possessing high dielectric constant is one of miniaturization strategies. The reflection coefficient is presented in Figure 27. The antenna resonates at 23.5GHz with a reflection coefficient of -26dB.

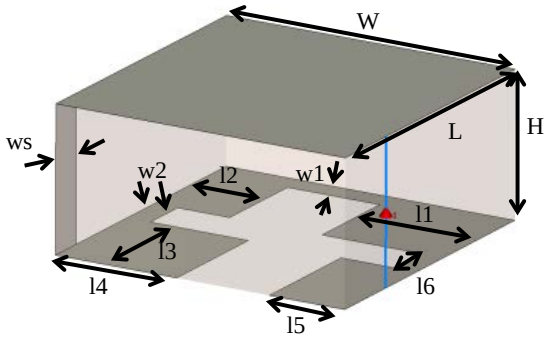

Figure 26. Design 1 and its parameters.

Table 7: Design 1 parameters.

Parameter	Value (mm)	Parameter	Value (mm)	Parameter	Value (mm)
L	2.50	l1	1.05	l5	0.65
W	2.50	l2	0.65	l6	0.40
H	1.00	l3	1.05	w1	0.20
ws	0.30	l4	1.05	w2	0.20

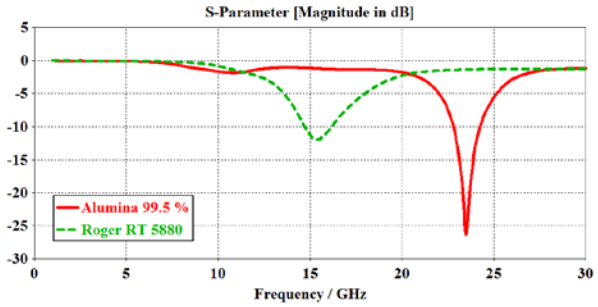

Figure 27. Reflection coeeficient of antenna with Roger RT 5880 and Alumina 99.5 % substrates.

The next step was replacing Alumina with Roger RT 5880 to observe to what extent the resonance frequency changes. Unexpected change was observed. It was believed that the resonance frequency should be shifted to higher values; however, the resonance frequency reduced from 23.5GHz to 15.42GHz with S_{11} changing from -25dB to -11.9dB at resonance frequency. Figure 27 shows the S_{11} change, which is presented by the green dashed line. Slots on the ground were designed to reduce the resonance frequency lower than 10GHz. The slots design is shown in Figure 26. Slots were created based on current density as seen in Figure 28. It can be observed that by increasing the current path from feed to the shorting pin and on the ground around the slots the resonance frequency is shifted to a lower value. Four cases were studied; case 1 and case 2 are for the antenna with Alumina 99.5% and Roger RT 5880, respectively. The antennas in these two cases do not have slots. Antenna having slots with Alumina 99.5% is referred to as case 3 and the one on with Roger RT 5880 is referred to as case 4.

Figure 29 shows the reflection coefficient of four cases. The slots, as expected, reduced the resonance frequency to lower values. Case 3 and case 4 have resonance frequencies at 6.41GHz and 6.09GHz, respectively. Nevertheless, case 4 has the best refection coefficient. Gain and radiation pattern were perceived in these four cases.

Table 8 lists the performance factors of antennas in each four cases in details. The gain was significantly reduced in case 3 and case 4, since the radiation efficiency degrades in these cases. To find the reason behind the reduction in efficiency power loss in different materials was studied (Figure 30). Power loss in skin at lower frequency is higher than the one at high frequency. Figure 31 shows that all four cases have significant cross polarization level. The E-field and H-plane locations were different in every case.

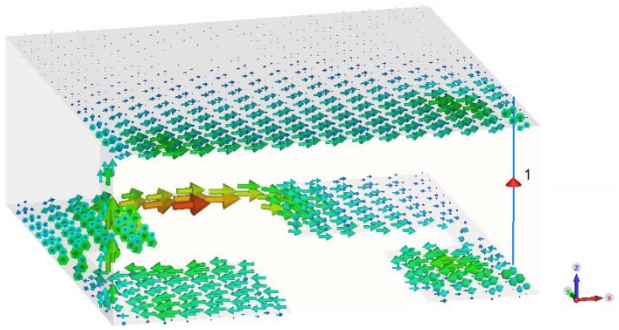

Figure 28. Current density on the ground.

It can be concluded that the power losses in skin were the reason for efficiency degradation. Also, in both cases of low and high permittivity high gain at lower frequency was not achieved; however, low dielectric substrate permittivity resulted in lower resonance frequency and better reflection coefficient. Although the antenna has good return loss at low frequency, the cross polarization is high.

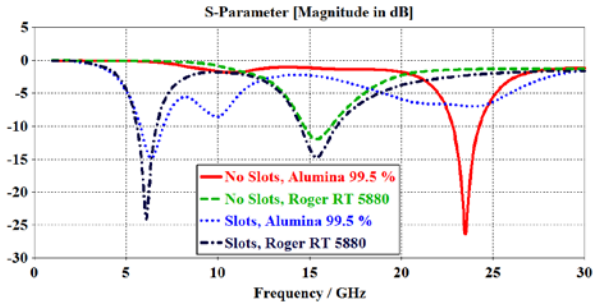

Figure 29. S_{11} before and after slots design with two substrates, Roger RT 5880 and Alumina 99.5%.

Table 8: Antenna performance in four cases.

Case	Name of the Case	Frequency GHz	Gain dBi	Efficiency (%)	Directivity dBi
1	No slots, Alumina	23.5	2.11	55.5	4.68
2	No Slots, Roger	15.4	0.32	54.6	3.23
3	Slots, Alumina	6.41	-16.4	1.23	2.92
4	Slots, Roger	6.09	-17.61	0.87	3.06

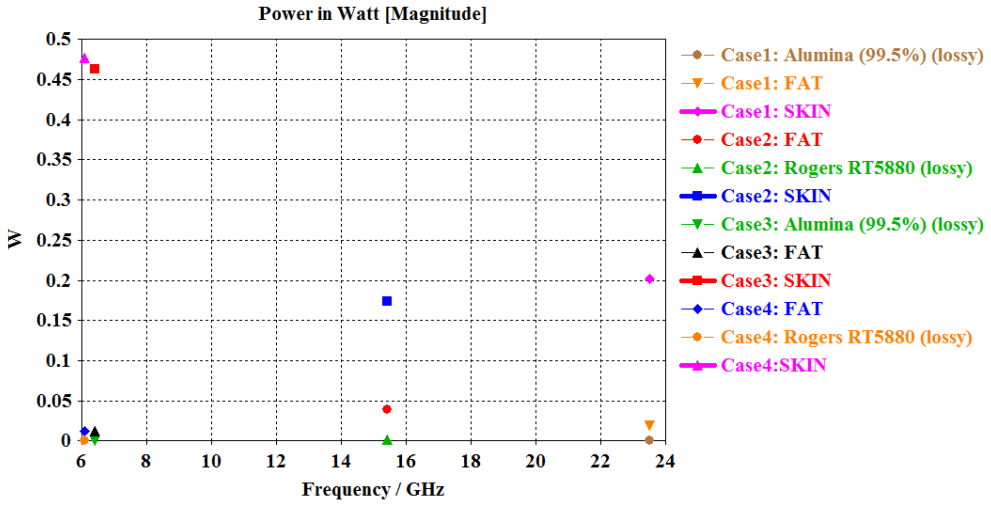

Figure 30. Power losses in materials.

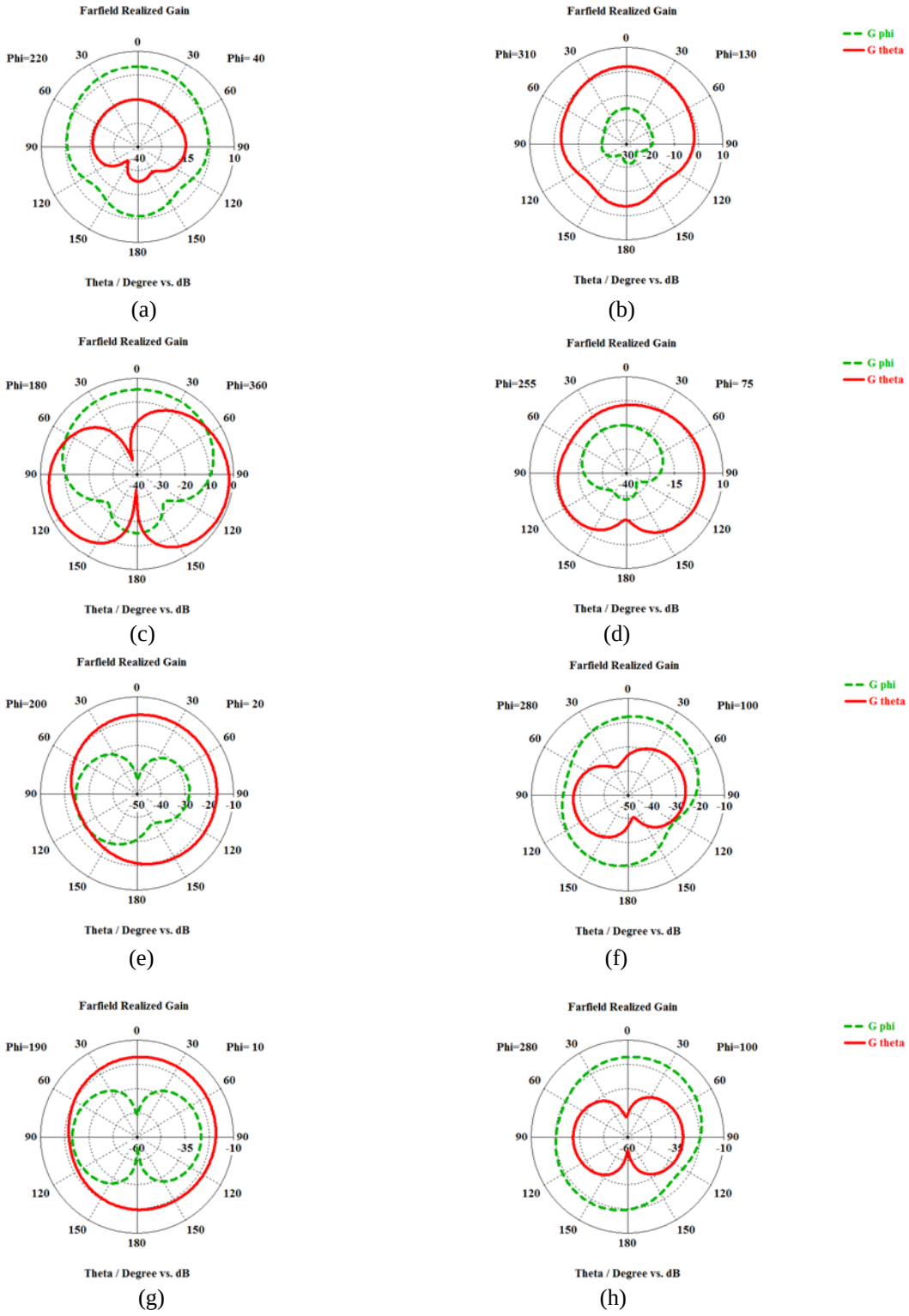

Figure 31. Radiation patterns: (a) and (b) case 1, (c) and (d) case 2, (e) and (f) case 3 , and (g) and (h) case 4.

3.3.3.2 *Design 2*

This design also started from a conventional PIFA. It was put above tissue layers and optimized until the new structure was obtained. The design is shown in Figure 32. The values of parameters are given in Table 9. Alumina 99.5%, and Roger RT 5880 were used for case 1 and case 2, respectively. The reflection coefficient and radiation patterns are depicted in Figures 33 and 34. Table 10 presents the performance of the antenna.

This antenna has a good performance at low resonance frequencies. The antenna works at resonance frequency of 7.2GHz with Alumina 99.5% as a substrate and 6.54GHz when Roger RT 5880 is used. As observed in the previous design, the resonance frequency with low dielectric substrate (Roger) is lower than the resonance frequency obtained from using high dielectric substrate (Alumina). It achieved a gain higher than the gain of design 1. Also, the antenna has good linear polarization, which can be observed from current density distribution that is mostly along x-axis on the patch and on the ground (Figure 35).

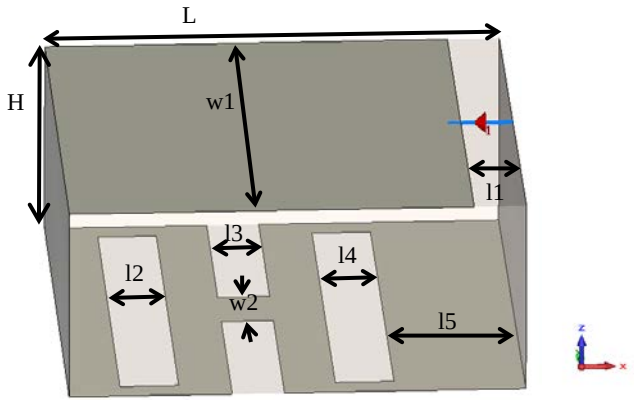

Figure 32. Design 2 with parameters.

Table 9: Parameters of design 2.

Parameter	Value (mm)	Parameter	Value (mm)	Parameter	Value (mm)
L	3.50	w2	0.50	l3	0.40
w1	3.50	l1	0.50	l4	0.45
H	1.5	l2	0.45	l5	1.00

Table 10: Antenna performance with two substrates, Alumina 99.5% and Roger RT 5880.

Case	Substrate	Frequency GHz	Gain dBi	Efficiency %	Directivity dBi
1	Alumina 99.5%	7.24	-9.79	4.83	3.46
2	Roger RT 5880	6.54	-11.2	3.07	3.91

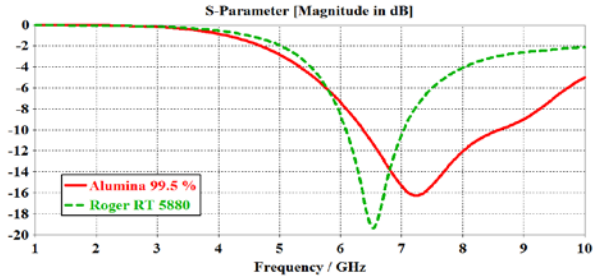

Figure 33. Reflection coefficient of design 2 with two different substrates.

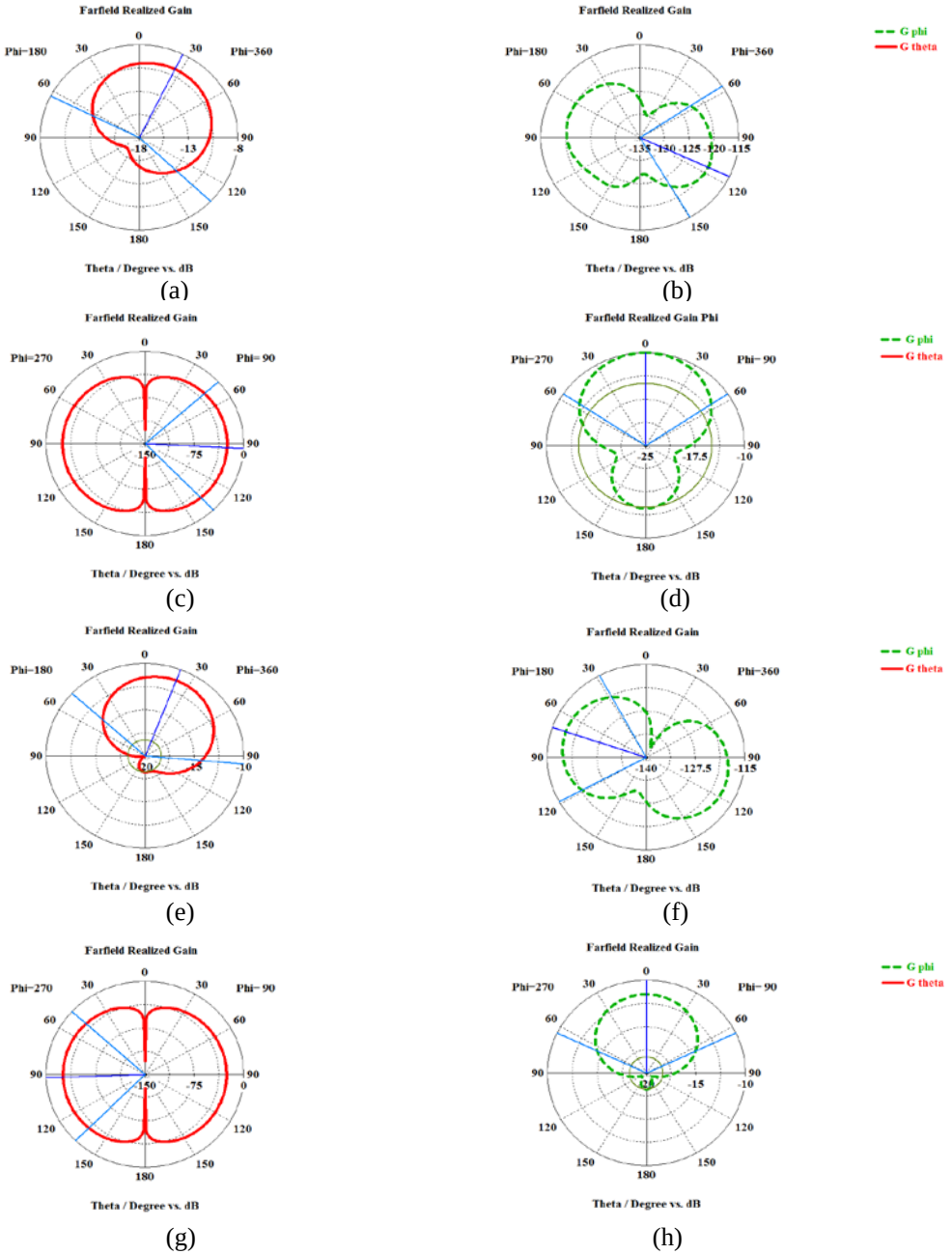

Figure 34. Radiation pattern of case1 (a)-(d), and case 2 (e)-(h).

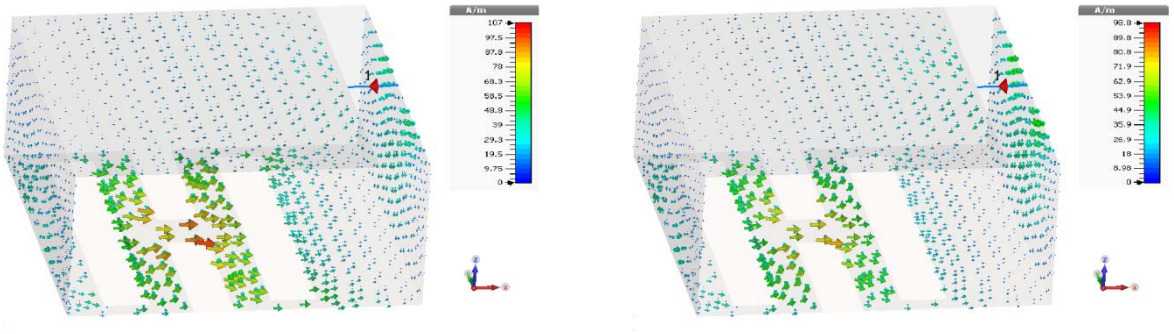

(a) (b)

Figure 35. Current density of design 2 with (a) Roger RT 5880 and, (b) Alumina 99.5% substrate.

The explanation of the slight higher gain with alumina 99.5% substrate is supported by three observations, which are the current density, the Smith chart of S-parameter, and the losses in the skin. The maximum current density in antenna with Alumina 99.5% substrate is 98.8 Ampere/meter, and the current associated with Roger RT 5880 is 107 Ampere/meter. This means the lower dielectric substrate leaks more current to the skin, which in turns increases the losses in skin. In Figure 36, the losses in the skin in case1 are slightly lower than the losses in the skin in case 2. The Smith chart as seen in Figure 37 shows that antenna in case1 is more capacitive than the antenna in case 2, because dielectric constant of Alumina is higher than Roger RT's.

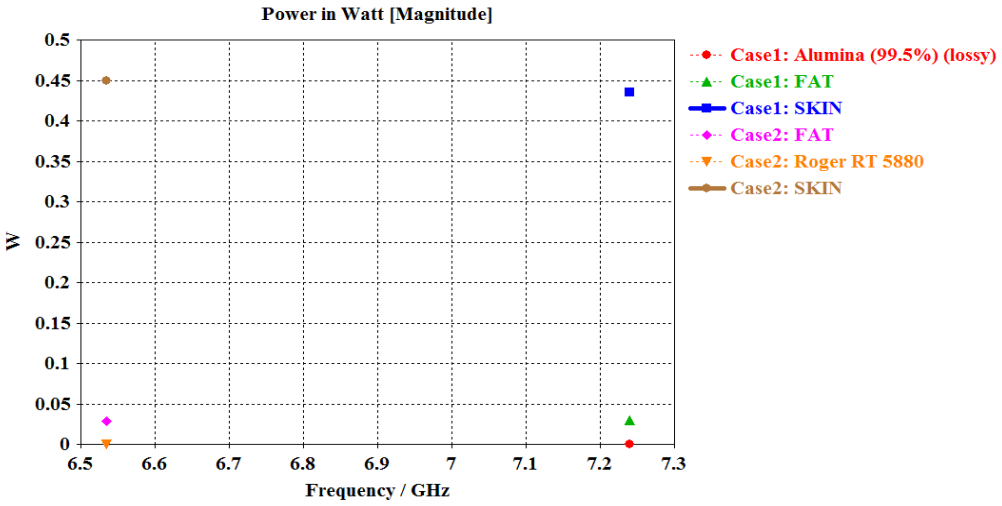

Figure 36. Losses in the tissue layers.

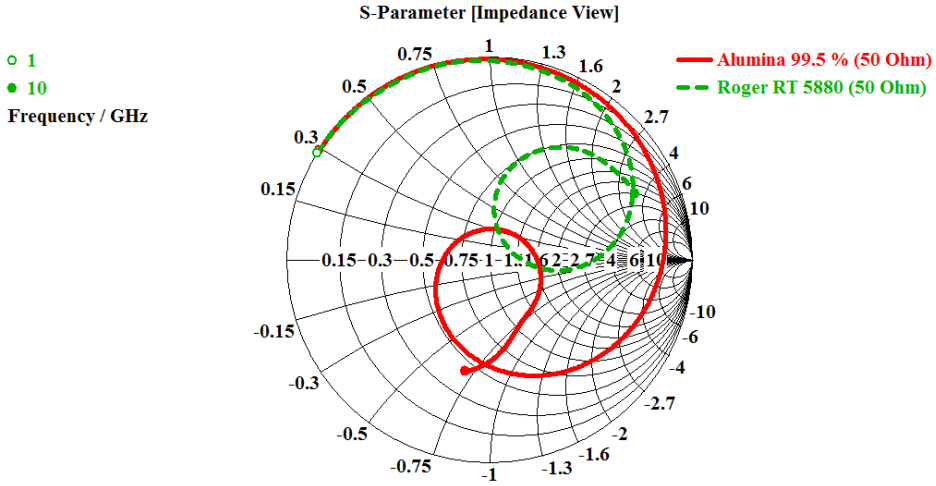

Figure 37. Smith Chart of S-parameter of case 1 and case 2.

3.3.3.3 *Design 3*

The third design is a modification of the second design. This design is shown in Figure 38, and its parameters are listed in Table 10. The substrate used for this antenna is Roger RT 5880. The antenna works at 3.65GHz and has a gain of -22dBi. The performance of the antenna is presented in Table 11 and Figure 39 shows the reflection coefficient.

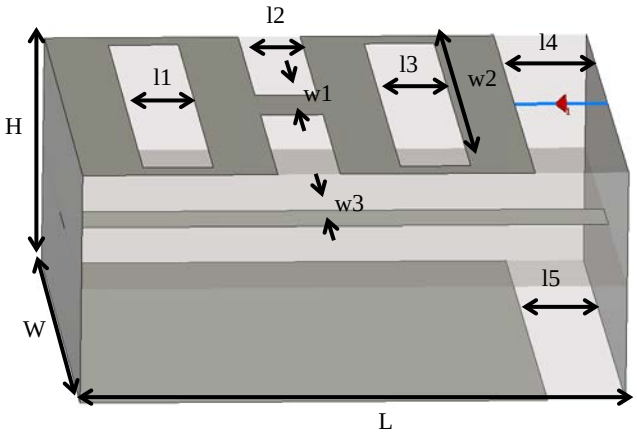

Figure 38. Design 3 and its parameters.

Table 11: Parameters of design 3.

Parameter	**Value (mm)**	**Parameter**	**Value (mm)**	**Parameter**	**Value (mm)**
L	3.50	w2	3.10	l3	0.45
W	3.50	w3	0.40	l4	0.50
H	1.50	l1	0.45	l5	0.50
w1	0.50	l2	0.40		

Table 12: Design 3 performance.

Substrate	**Frequency GHz**	**Gain dB**	**Efficiency (%)**	**Directivity dBi**
Roger RT 5880	3.65	-21.9	0.36	2.58

The shape of antenna is unique. The major elements in antennas are the strip in the middle and the gap between the ground and the conductive layer attached to the skin (Figure 40); removing one of these elements, or connecting the conductive layer to the ground causes degradation in the antenna's performance. The strip and the conductive layer have most of the current density, which results in linear polarized radiation (Figures 41). The low gain values are caused by the same effect mentioned in the previous section: the skin loss effect. However, it was discovered that the gain gradually enhances when the surface area of the tissue increases with slight reduction in resonance frequency. Table 13 shows the gain variation with different surface areas and Figure 42 depicts the reflection coefficient variation. The efficiency increases with increase in the surface area. However, the variation of the directivity is not predictable.

The antenna was lifted up so it was not attached to the skin. Then the variation of the resonance frequency and the antenna performance with different surface areas was observed. The air gap between the skin layer and the antenna was from 0.1mm to 1mm. the performance of the antenna with different surface areas and elevation is summarized in Table 14. In general, it was observed that once the antenna is not attached to the skin, the resonance frequency moved to higher values, in the range of 8GHz to 11GHz. Another observation is that the gain and the efficiency increase sharply from around -20dBi to above zero dBi. Nevertheless, a slight increment was seen in in the directivity.

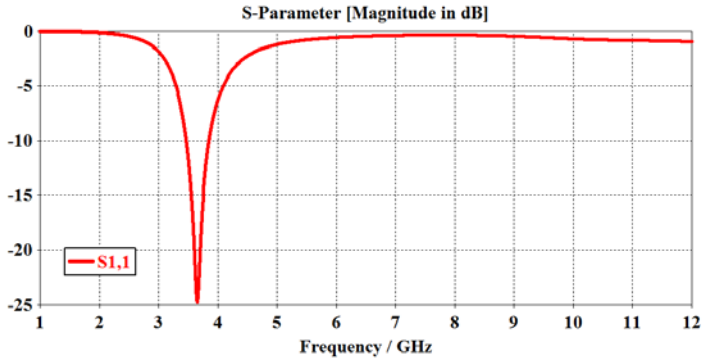

Figure 39. Reflection coefficient of design 3.

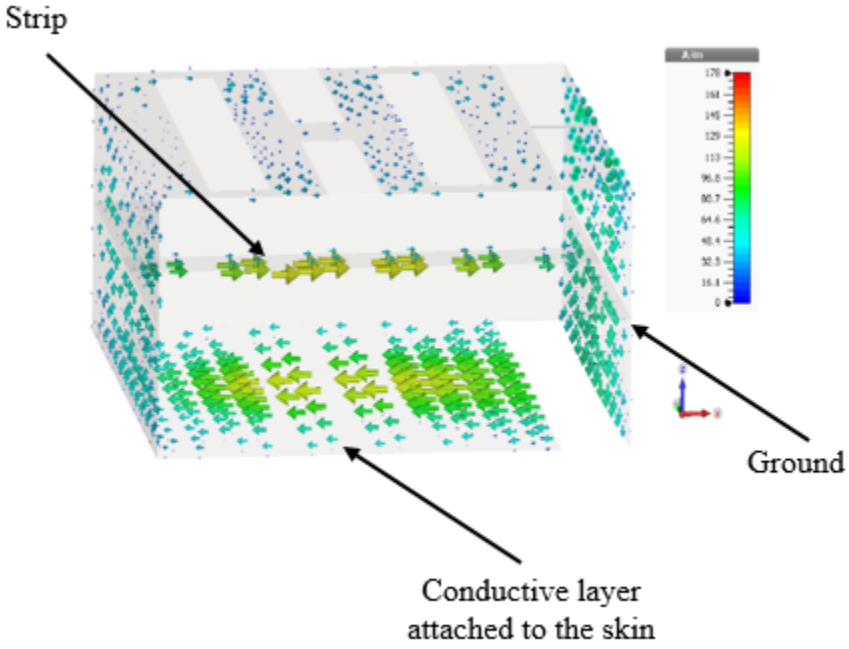

Figure 40. Current density of design 3.

Table 13: Antenna performance with surface area variation.

Case	Surface area	Frequency GHz	Gain dBi	Efficiency (%)	Directivity dBi
1	5 x 5 mm^2	3.66	-21.87	0.36	2.57
2	10 x 10 mm^2	3.54	-20.39	0.50	2.64
3	20 x 20 mm^2	3.51	-17.94	1.26	1.07

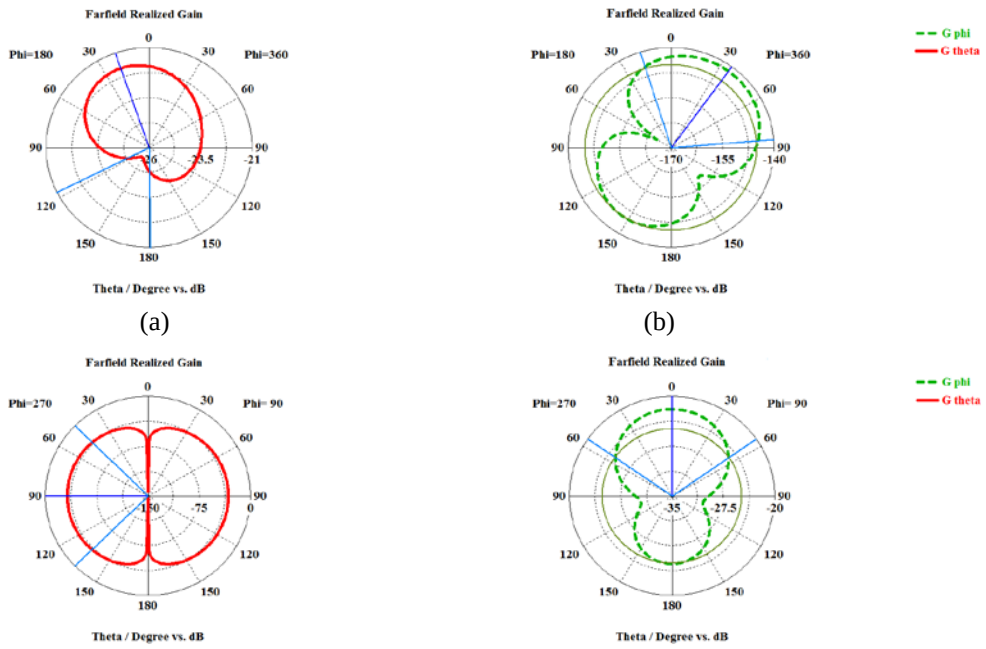

Figure 41. Radiation patterns of design 3.

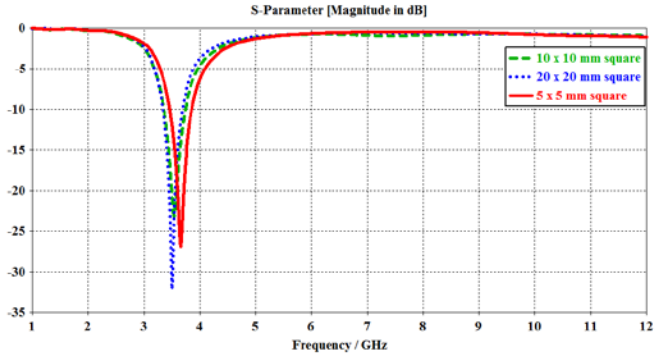

Figure 42. Reflection coefficient variation with different surface areas of tissues.

Table 14: Antenna performance with different elevation and different surface areas.

Surface area (mm^2)	***5 x 5***					
Case	**Air gap above the skin (mm)**	**Frequency (GHz)**	**S_{11} (dB)**	**Gain (dBi)**	**Efficiency (%)**	**Directivity (dBi)**
1	0.0	3.66	-25.9	-21.87	0.36	2.57
2	0.1	8.70	-8.50	-2.592	43.8	2.04
3	0.5	10.21	-9.51	-0.196	69.8	1.88
4	1.0	10.62	-8.43	0.228	79.3	1.88
Surface area (mm^2)	***10 x 10***					
Case	**Air gap above the skin (mm)**	**Frequency (GHz)**	**S_{11} (dB)**	**Gain (dBi)**	**Efficiency (%)**	**Directivity (dBi)**
1	0.0	3.54	-22.8	-20.39	0.50	2.64
2	0.1	8.59	-10.6	-1.637	42.8	2.43
3	0.5	10.17	-16.3	-0.294	59.3	2.08
4	1.0	10.58	-14.0	0.727	66.1	2.70
Surface area (mm^2)	***20 x 20***					
Case	**Air gap above the skin (mm)**	**Frequency (GHz)**	**S_{11} (dB)**	**Gain (dBi)**	**Efficiency (%)**	**Directivity (dBi)**
1	0.0	3.51	-21.0	-17.94	1.26	1.07
2	0.1	8.58	-11.6	-1.716	41.2	2.45
3	0.5	10.16	-14.5	1.803	54.8	4.57
4	1.0	10.54	-12.9	3.165	63.7	5.37

CHAPTER 4 STUDY OF MINIATURIZED ANTENNA ON HUMAN HEAD MODEL

In this chapter, we focus on the application of a miniaturized antenna related to human brain. In many applications such as brain imaging and brain signal monitoring, it is required to place antennas on the head. Design 3, which was provided in Chapter 3, was chosen to be studied when it was placed on tissue layers mimicking human head. Breast and head layers are different. Breast has fat under the skin with noted thickness and low dielectric properties. On the other hand, the head layers do not possess fat, but there are scalp and brain tissue layers under the skin that have higher dielectric properties than skin.

Design 3 was slightly modified as depicted in Figure 43 and its parameters are listed in Table 15. The antenna was mounted on layers of head tissues as well as a realistic head model as shown in Figures 44-45.

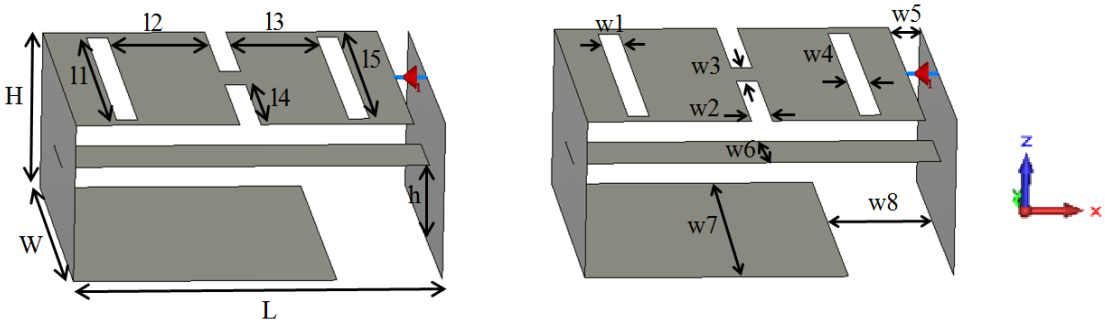

Figure 43. Design 3 with modification.

Table 15: Antenna dimensions.

Parameter	Value (mm)	Parameter	Value (mm)	Parameter	Value (mm)
L	3.50	l3	0.85	w4	0.20
W	3.50	l4	1.50	w5	0.30
H	1.50	l5	3.10	w6	0.80
h	0.75	w1	0.20	w7	3.50
l1	3.10	w2	0.20	w8	1.00
l2	0.95	w3	0.50		

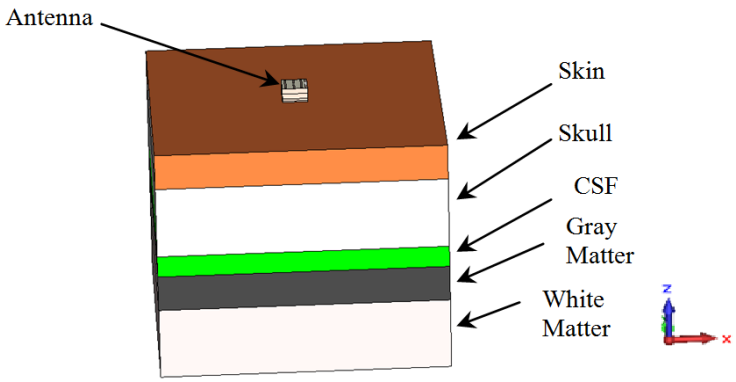

Figure 44. Antenna on head tissue layers.

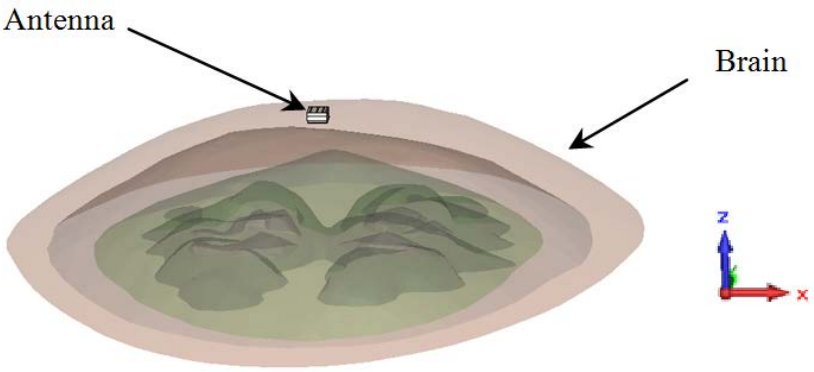

Figure 45. Antenna mounted on realistic head model.

The realistic head model provided by Professor A. Sabouni, was obtained using three-dimensional (3D) Magnetic Resonance Imaging (MRI) data from a 25 year-old healthy human subject. The head layers are scalp, skull, Cerebro-Spinal Fluid (CSF), Gray Matter (GM), and White Matter (WM). The dielectric properties values were assigned to each tissue type. Dielectric properties of head tissue were modeled using the second order Debye model. The dielectric parameters were obtained from [39] except for the CSF parameters that were not provided in [39]. We calculated the average value of CSF dielectric properties at 1 GHz and 10 GHz, obtained from [40], Table 16 provides the Debye model parameters and Table 17 presents the calculated average value of CSF.

Table 16: Debye parameters of head tissue.

Tissue type	ε_∞	ε_{S1}	ε_{S2}	τ_1 **(ps)**	τ_2 **(ns)**	**Height (mm)**
Skull	4.31	20.43	24.0	10.80	0.46	10
GM	6.37	49.78	85.96	7.52	0.69	5
WM	5.74	36.73	46.48	7.54	0.54	10
Skin	4.39	37.16	70.17	7.42	0.57	5

Table 17: Dielectric properties of Cerebrospinal Fluid (3mm thickness).

Tissue	**Permittivity (ε_r)**		**Conductivity (σ)**		ε_{rave}	σ_{rave}
Frequency (GHz)	1	10	1	10	60.40	8.90
CSF	68.40	52.40	2.45	15.37		

4.1 Antenna Performance in Free-Space

The antenna resonates at 15.88GHz as shown in Figure 46. Figure 47 shows that the current density is mostly on the strip in the middle of the antenna. The antenna is linearly polarized. Co-polarized field components are E_θ on $\phi=0^o$ and $\phi=180^o$ (E-plane) and E_φ on $\phi=90^o$ plane (H-plane). Since the cross-polarization level is very low the total gain has been shown in Figure 48 and the cross-polarized fields are not separated from co-polarized fields.

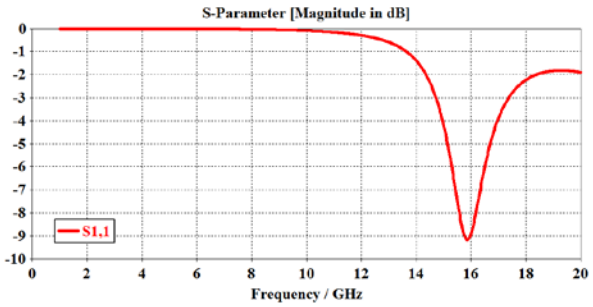

Figure 46. Reflection coefficient of the proposed antenna in free-space.

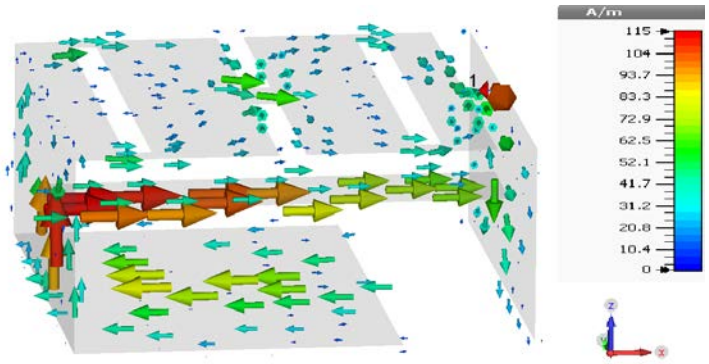

Figure 47. Current density of antenna in free-space.

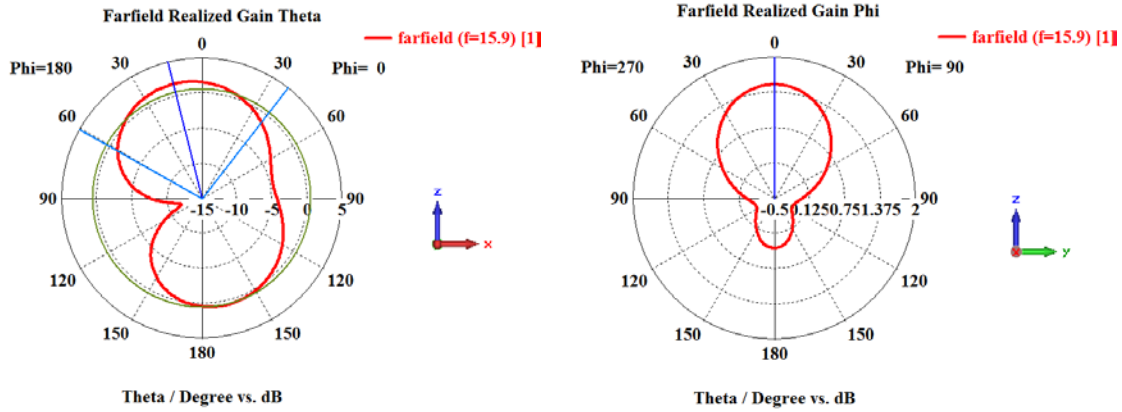

Figure 48. E-plane and H-plane gain patterns in free-space.

4.2 Antenna Performance on Human Head Model

The antenna was simulated on a model of human head tissue layers. Three surface areas were chosen. Figure 49 depicts these models with the surface areas of 2x2cm^2, 4x4cm^2, and 6x6cm^2. The simulations were also done when the antenna was placed on the MRI driven segmented head model. It is known that the head tissues have significant loading impact on the antenna's performance, therefore, it was necessary to estimate these effects using a less computational layer models. One major question was how big of the surface area in a layered model was necessary to include the most significant loading

effects in the simulation. This could help to make a decision on the size that is needed from segmented head model to have an accurate simulation.

By comparing Figures 46 and 50 it can be observed that the resonance frequency has shifted from 15.88GHz (in free-space) to 4.06GHz when antenna was placed on head models. The shift in resonance frequency, as explained in [3], is due to skin's high permittivity in the vicinity of the antenna. In such situations skin becomes a part of antenna and increases the effect permittivity of the substrate. Thus, the resonance frequency is shifted to a lower value. It is clear from Figure 50 that the surface size of the area did not cause any difference in the reduction of frequency, as all cases show the same resonance frequency at 4.06GHz.

The radiation patterns, however, are very much affected by the surface area. The radiation patterns of four cases are presented in Figure 51 and the changes in gain levels are highlighted in Table 17. Co-polarized components are G_θ (ϕ=0) (E-plane) and G_ϕ (ϕ=90^o) (H-plane). As stated in Table 18, the gain drops significantly due to tissue losses. The radiation patterns also become more directive in the E-plane, as the surface area is increased to 4x4cm^2. Consequently, we concluded that 4x4cm^2 of the surface area would be sufficient to include the loading effects.

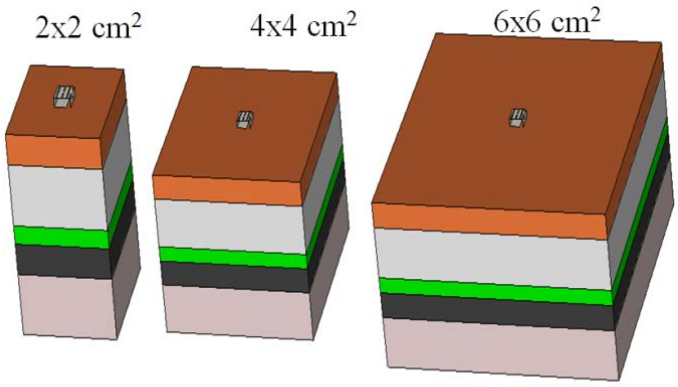

Figure 49. Antenna mounted on layered model with three surface areas.

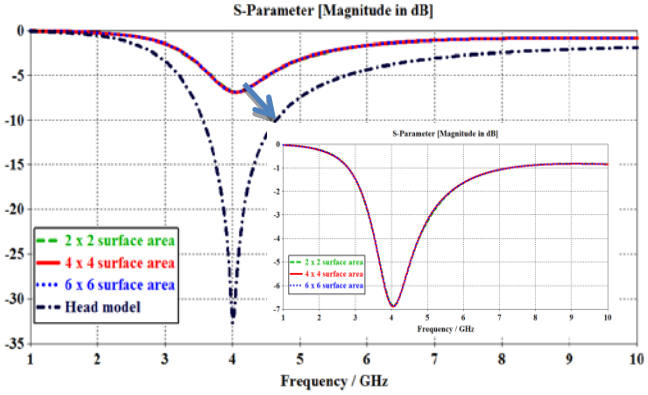

Figure 50. Reflection coefficient of antenna on three layered models and a realistic head model.

Table 18: Antenna gain in different planes on different layers

Case	G_θ (ϕ=0)	G_ϕ (ϕ=0)	G_θ (ϕ=90)	G_ϕ (ϕ=90)
Free-space	1.7	-107.0	-8.5	1.5
2x2cm^2	-17.5	-137.0	-35.1	-17.6
4x4cm^2	-17.9	-134.0	-37.3	-18.0
6x6cm^2	-16.2	-136.0	-37.4	-16.3
Head model	-16.2	-44.4	-34.2	-16.2

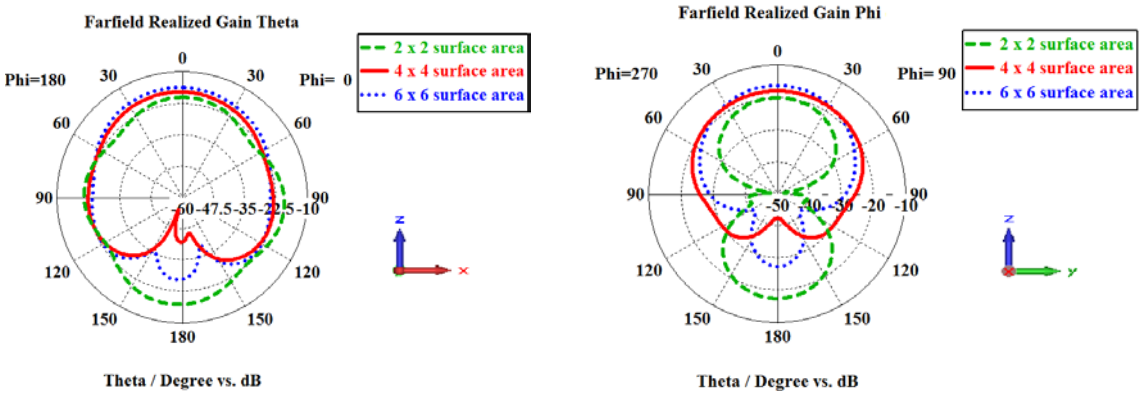

Figure 51. E-plane(left) and H-plane (right) gain patterns on tissue layers.

4.3 Antenna Performance Enhancement

Since the gain is very low, further performance enhancement is needed. Two techniques were performed to improve the performance of the antenna. First, the reflection coefficient of the antenna was enhanced by replacing the air substrate with a high dielectric layer. The chosen substrate was Alumina (99.5%) (ε_r=9.9, tanδ =0.0001). The reflection coefficient of the antenna after addition of Alumina substrate for the case that antenna is placed on a layer model with 4x4cm^2 is depicted in Figure 52.

The resonance frequency dropped from 4.06GHz to 3.80GHz. However, there was no change in the gain due to skin layer loading effects (case 1 in Figure 52 (a)). To improve the gain, the antenna was elevated by 0.1mm, 0.5mm and 1mm above the skin. These cases are referred to as case 2-case 4, respectively, in Figures 52-53. Adding the air gap improved the gain significantly, while it did not change the radiation patterns, and the reflection coefficient is still less than -10dB at the center frequency. However, it caused a significant increase in the resonance frequency, as shown in Table 19. The same procedure was done for antenna above the segmented head model. Please note that for

these simulations we had to reduce the mesh size and accuracy due to the size of numerical calculations. The reflection coefficients and gain levels are summarized in Figure 52(b) and Table 20, respectively. The results of resonance frequencies are very similar to 4x4cm^2, while the gain shows some reduction. We conclude that the layered model is a good approximation of full segment model of head when doing quick simulations.

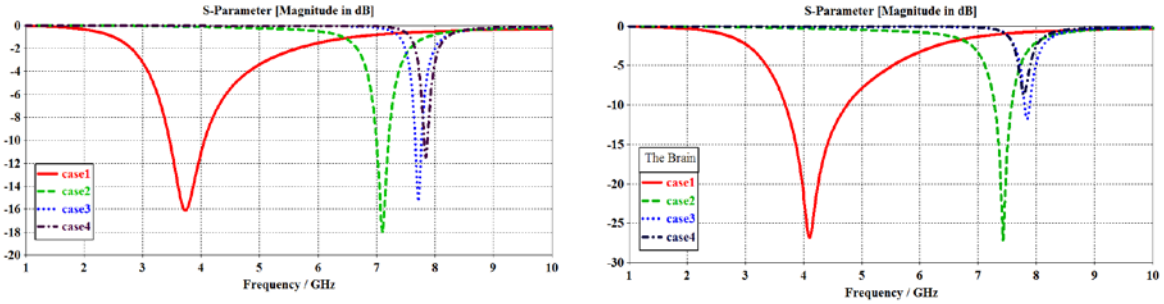

(a) (b)

Figure 52. Reflection coefficient for different cases on (a) 4x4cm^2 layered model, and (b) head model. The cases refer to different spacing as listed in Tables 19 and 20.

Table 19: Antenna gain for various spacing above a 4x4cm^2 layered model, S is the spacing, f_r is the resonance frequency.

Cases	S (mm)	G_θ (ϕ=0)	G_ϕ (ϕ=0)	G_θ (ϕ=90)	G_ϕ (ϕ=90)	f_r (GHz)
1	0.0	-17.9	-134	-38.8	-17.90	3.75
2	0.1	-3.1	-113	-13.2	-3.35	7.10
3	0.5	0.1	-110	-11.0	0.05	7.72
4	1.0	1.4	-109	-11.1	1.36	7.84

Table 20: Antenna gain for various spacing above a head model, S is the spacing, f_r is the resonance frequency.

Cases	S (mm)	G_θ (ϕ=0)	G_ϕ (ϕ=0)	G_θ (ϕ=90)	G_ϕ (ϕ=90)	f_r (GHz)
1	0.0	-14.8	-43.0	-32.2	-14.8	4.10
2	0.1	-4.15	-28.4	-16.0	-4.17	7.43
3	0.5	-0.29	-23.2	-9.93	-0.38	7.85
4	1.0	0.36	-23.5	-10.5	0.29	7.79

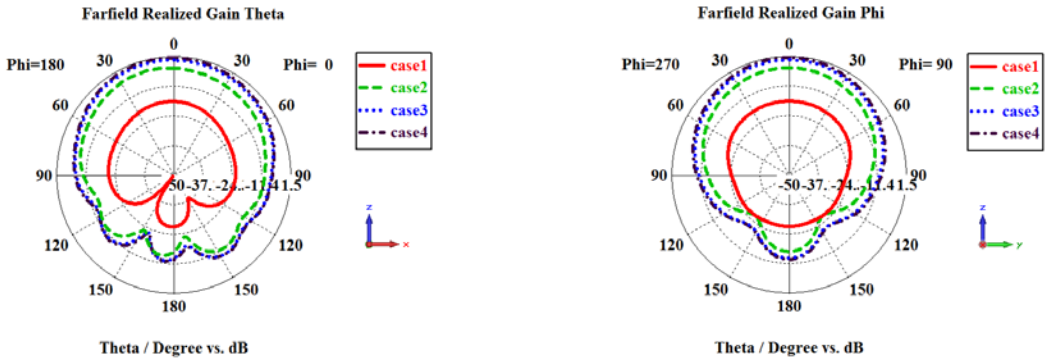

Figure 53. E-plane (left) and H-plane (right) radiation patterns of cases as listed in Table 19.

4.4 Specific Absorption Rate

The Specific Absorption Rate (SAR) is the radiation that is absorbed by the tissue. The maximum SAR limit according to IEEE standards is 1.6W/kg for 1g of tissue. To comply with this standard, the input power of the antenna, when it is placed 0.5mm above head, has to be less than 0.257W. Fig. 55 shows the SAR value after power was reduced.

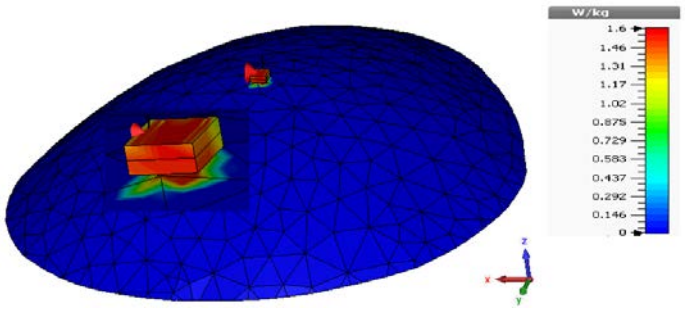

Figure 54. SAR distribution on head model.

CHAPTER 5 FABRICATION AND EXPERIMENTAL RESULTS

5.1 Introduction

Fabrication and testing of miniaturized antennas imposes many challenges. First challenge is the vicinity of skin layer to the antenna that can result two problems. First, when the antenna is slightly lifted up, e.g. 0.1mm from skin layer, the resonance frequency shifts to higher values, which makes the resonance frequency of the antenna unpredictable. Another problem is that keeping the distance between antenna and skin layer is difficult and will require additional structures. It is of interest to find a solution to these issues and design an antenna that can work at lower frequencies and does not depend greatly on the spacing between the body and antenna. Therefore, the possibility of using magneto-dielectric layers to overcome these issues is investigated in this chapter.

The major challenge in fabrication arises from the small dimensions and resolution needed in fabrication of the antenna. Therefore, optimizations were performed to keep the dimensions ranging from 0.5mm to 3.5mm, while keeping the resonance frequency below 6GHz, and good performance.

In previous chapters, all the simulations have been done on planar tissue layers. In real setting antennas might be placed on curved surfaces of the body. The antenna was tested on curved tissue layers to perceive if there is a change in the antenna performance.

5.2 Antenna Performance on Magneto-Dielectric Substrate

5.2.1 Introduction

The idea initially was to design a structure beneath the antenna that has similar characteristic to the skin and isolates the antenna from the tissue layers to reduce the losses. However, it was observed that using magneto-dielectric material substrate can provide both the supporting structure as well as stabilizing the resonance frequency.

Addition of the magneto-dielectric substrate to the antenna moved the resonance frequency to around 5GHz, while antenna was either in free-space or placed on tissue layers with different spacing from the tissue layers. In another word, it made the antenna's resonance frequency independent from the distance from tissue layers. In addition, the tissue layers support the antenna performance; they enhance the outward radiation direction and increase the gain of the antenna without changing the resonance frequency.

5.2.2 Antenna Design and Performance on Magneto-Dielectric Substrate

Design 3 from Chapter 3 with slight modification was studied. The first substrate used was Roger RT 5880. Nine cases were observed to get a general view on the influence of tissue layers on the resonance frequency of the antenna. The antenna parameters are shown in Figure 55. Table 21 lists the dimension of the antenna. The first idea was designing a material that has similar properties to the skin to make the performance of the antenna independent from the tissue layers effect (Figure 56). Figure 57 shows the reflection coefficient for two different cases. This figure shows that there is minimal change in the resonance frequency when the antenna is placed 1mm above the

layers or in free-space. The antenna resonates with good reflection coefficient and bandwidth at 6.38GHz and 6.25GHz in free-space and on 400mm^2 surface area layers, respectively.

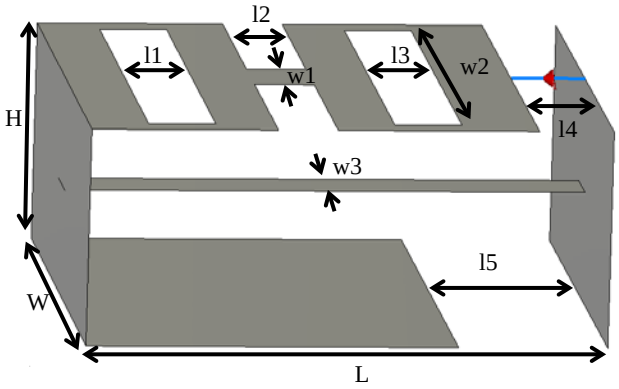

Figure 55. Modified antenna from design 3 (Chapter 3).

Table 21: Modified antenna 3 dimension.

Parameter	Value (mm)	Parameter	Value (mm)	Parameter	Value (mm)
L	3.50	w2	3.10	l3	0.45
W	3.50	w3	0.40	l4	0.50
H	1.50	l1	0.45	l5	1.00
w1	0.50	l2	0.40		

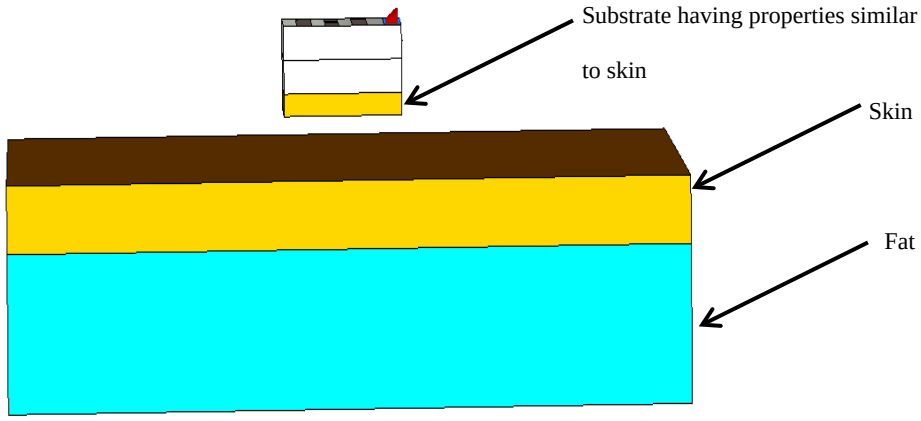

Figure 56. Antenna with a substrate with similar properties to skin dielectric properties is placed 1mm above skin and fat layers with the area of 400-mm^2.

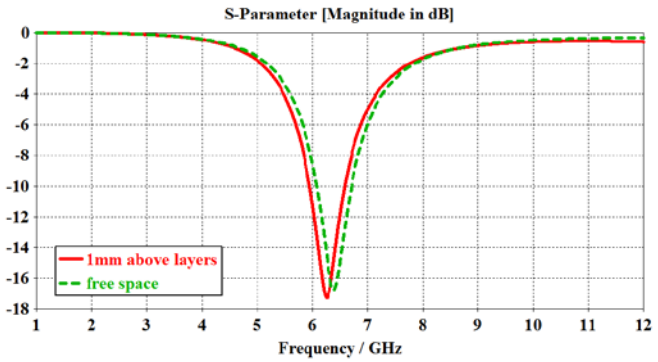

Figure 57. Reflection coefficient of antenna in free-space and placed1mm above layers.

A study in [41] shows that a substrate that has permeability higher than 1 can be utilized to reduce the antenna size and improve impedance matching and radiation performance. The magneto-dielectric was modeled and tested in CST simulation. The dielectric and magnetic parameters are presented in Table 22; since the properties in [41] are values measured from 1 MHz to 1 GHz, the substrate was modeled at 500MHz.

Table 22: Dielectric and magnetic properties of the substrate.

Property	Value	Property	Value
ε'	12.0	μ'	2.00
$\tan\theta = \varepsilon''/\varepsilon'$	0.01	$\tan\theta = \mu''/\mu'$	0.38

Nine cases, as depicted in Figure 58, were examined. Figure 59(a) which depicts cases 1-3 proves that the tissue layers have a significant effect on antenna resonance frequency. From case 1 to case 2, the antenna is lifted 1mm above the layers which results in a sharp increment in the resonance frequency, beyond 12GHz. Similarly, the resonance frequency of the antenna in free-space is shifted up.

The magneto-dielectric substrate provides a promising solution for the antenna design. It reduces the resonance frequency. When the antenna is placed on the layered

model, case 4, the resonance frequency is 3.25GHz, which is lower than the resonance frequency of case 1. Figure 59(b) shows that 1mm space between the antenna and the skin layer shifts the resonance frequency from 3.25GHz to 5.9GHz which is much lower the frequency shift observed in the first three cases. However, the resonance frequency variation should be minimized further.

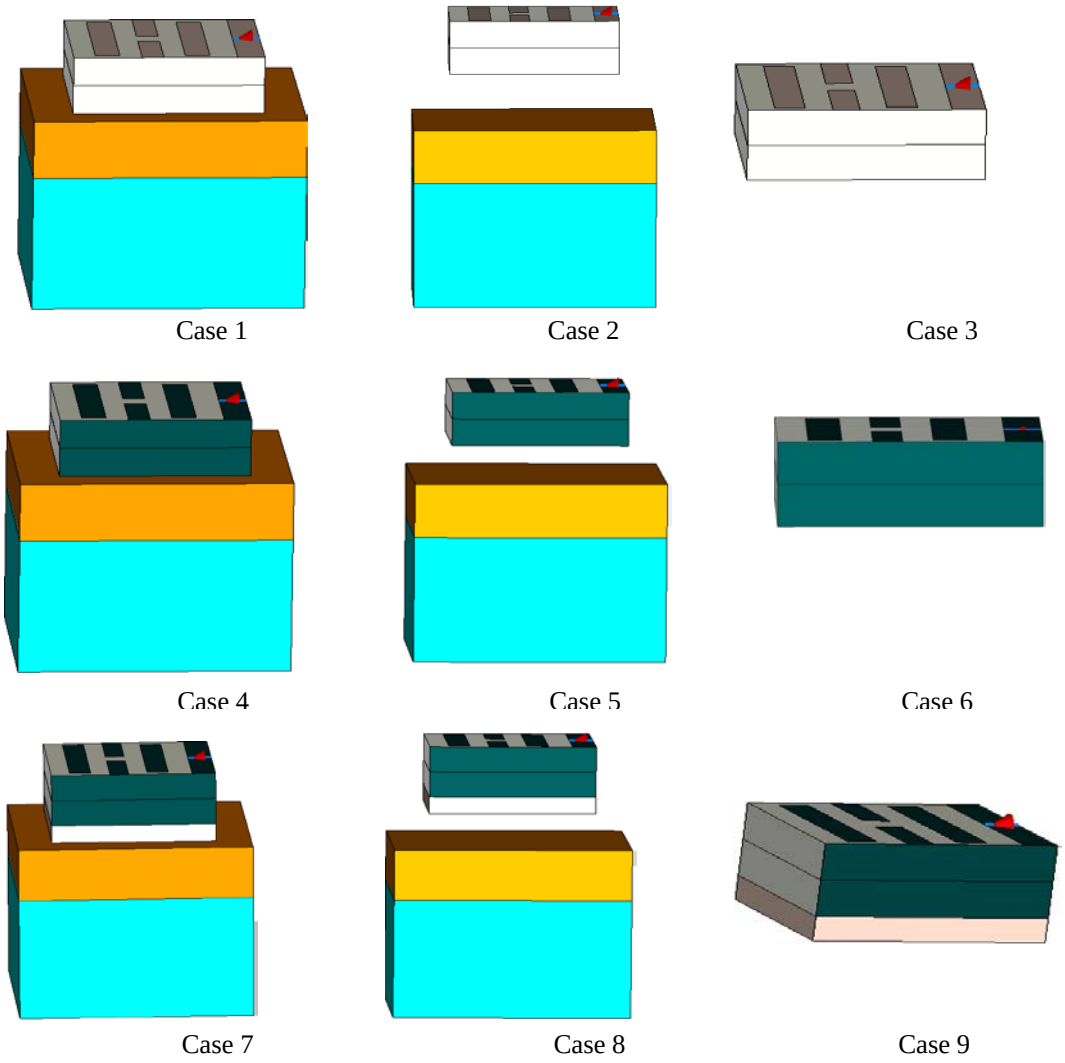

Figure 58. Nine cases to isolate the antenna from tissue layers.

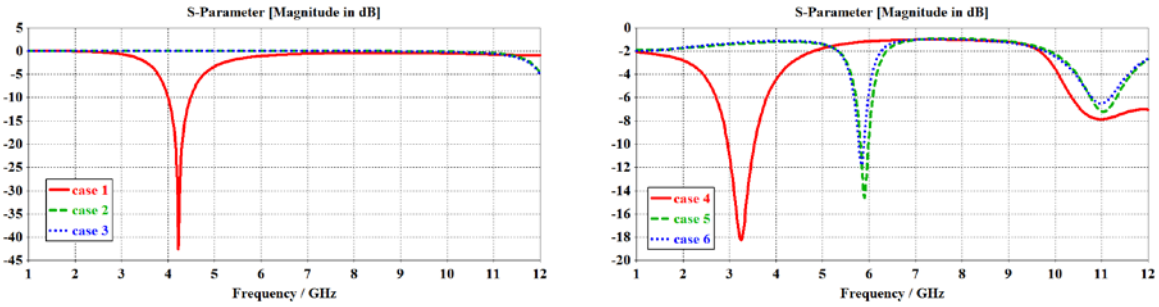

(a) (b)

Figure 59. Reflection coefficient of (a) cases1-3, (b) cases 4-6.

Adding a dielectric substrate beneath the antenna helps to stabilize the resonance frequency and make it independent from the tissue layers. For case 7 Alumina 99.5% was placed under the antenna and the reflection coefficient was obtained while the antenna was placed on the tissue layers. Case 8 shows the same setup after adding 1mm air-gap, and case 9 shows the same antenna in free-space. We assumed that the high dielectric constant material reduced the influence of frequency shits, since the difference in dielectric value of the tissue and Alumina are different. The reflection coefficient of these cases is shown in Figure 60. As it is expected, the variation of the resonance frequency from case 7 to case 8 was extremely reduced. Furthermore, the resonance frequency of case 8 and case 9 are almost the same.

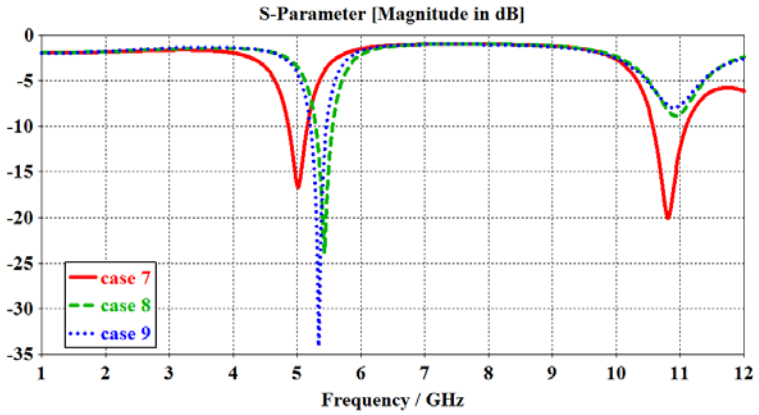

Figure 60. Reflection coefficient of cases 7-9.

The performance of the antenna in nine cases is presented in Table 23. Please note that the results of cases 2 and 3 are not provided since their resonance frequencies are out of range of interest, which is below 10GHz. Moving the antenna away from the layers improves the performance. From Table 23 it can be observed that case 1 and case 4 show the losses in tissue layers are significant, which degrades the radiation efficiency. Nonetheless, the efficiency to some extent increases by placing a substrate layer between the antenna and the skin layer. This is shown in case 7. In cases 8 and 9, the gain was increased to around -13 dBi, which is below -10dBi. As seen in previous section, the gain could be enhanced when surface area of tissue layers increases.

Table 23: Performance of the antenna in nine cases.

Case	Frequency (GHz)	Gain (dBi)	Efficiency (%)	Directivity (dBi)
1	4.23	-18.8	0.71	2.69
2	----	----	----	----
3	----	----	----	----
4	3.26	-23.0	0.26	2.89
5	5.89	-12.2	3.49	2.52
6	5.84	-12.6	3.23	2.59
7	5.02	-13.8	2.85	1.70
8	5.43	-13.0	3.06	2.14
9	5.34	-13.4	2.68	2.34

The gain and radiation pattern behavior with different surface area sizes are similar to ones reported for the head model. The performance of the antenna in free-space and different area sizes with 1mm air-gap are listed in Table 24, and the radiation patterns are depicted in Figure 61.

The gain was enhanced from -13.4dBi to -7.9dBi by increasing the surface area. Also, an increase in the efficiency was noted. However, the directivity was affected with changes in the surface area size. The radiation patterns have similar behavior to the patterns for the case of head model. The co-polarization patterns, the gain pattern along x-axis and gain along y-axis, are more directive towards the broadside direction as the surface size is increased.

In conclusion the magneto-dielectric substrate has positive effects on the antenna performance. It keeps the resonance frequency less affected by the distance from the tissue layers.

Table 24: Performance of the antenna on different surface area with 1mm gap.

Surface Area (mm^2)	**Frequency (GHz)**	**S_{11} (dB)**	**Gain (dBi)**	**Efficiency (%)**	**Directivity (dBi)**
Free space	5.34	-33.6	-13.4	2.67	2.34
5 x 5	5.43	-23.8	-13.0	3.08	2.14
10 x 10	5.41	-26.9	-10.9	3.73	3.39
20 x 20	5.42	-37.1	-7.9	8.31	2.84

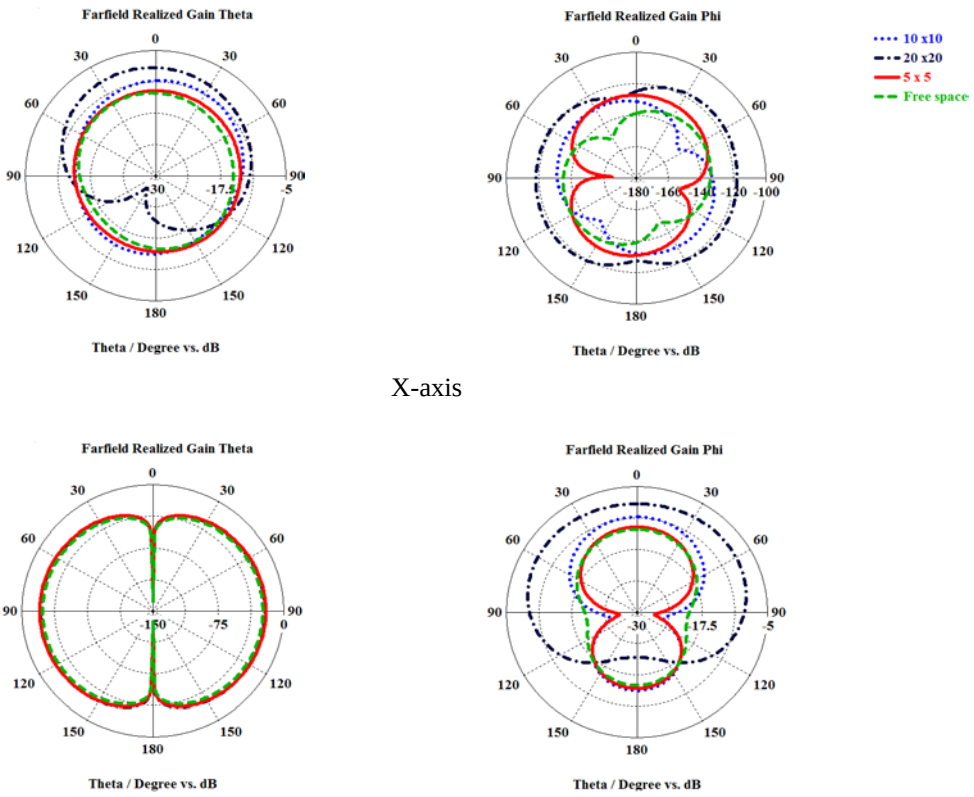

Figure 61. Radiation patterns with different surface area sizes.

5.3 Dimension Optimization with Fabrication Considerations

5.3.1 Introduction

The major issue of the previously proposed antennas was the limited resolution of the milling machines that makes it very expensive to fabricate antennas with dimensions under 0.5mm. Optimizations were performed to modify the antenna dimensions from 0.5mm to 3.5mm with keeping the resonance frequency below 6GHz.

5.3.2 Antenna Designs and Performance

There are two optimized antennas designs derived starting from design 3 (Chapter 3). The two optimized antennas are shown in Figure 62, and there dimensions are listed

in Tables 25-26, respectively. The second optimization was performed to limit the shortest dimension to 1mm. The orientation of the feed was changed for easier transmission line designs. The material used as a substrate in this study is the magneto-dielectric.

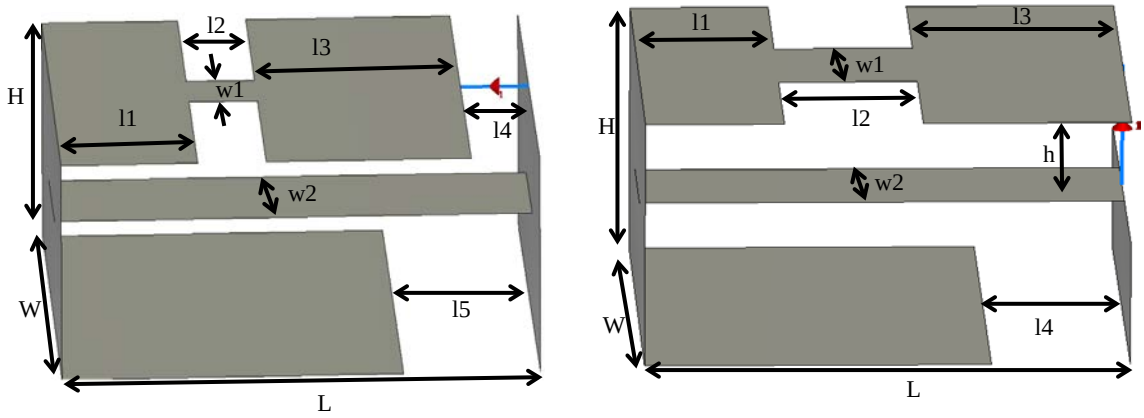

(a) (b)

Figure 62. (a) Optimized antenna 1, and (b) optimized antenna 2.

Table 25: Dimensions for first optimized antenna.

Parameter	Value (mm)	Parameter	Value (mm)	Parameter	Value (mm)
L	3.50	w2	1.00	l4	0.50
W	3.50	l1	1.00	l5	1.00
H	1.50	l2	0.50		
w1	0.50	l3	1.50		

Table 26: Dimensions for second optimized antenna.

Parameter	Value (mm)	Parameter	Value (mm)	Parameter	Value (mm)
L	3.50	w2	1.00	l4	1.00
W	3.50	l1	1.00	h	1.00
H	2.00	l2	1.00		
w1	1.00	l3	1.50		

The reflection coefficient of these two optimized antennas is shown in Figure 63. After first optimization, the resonance frequency shifted from 5.43GHz to 5.64GHz, and the reflection coefficient at center frequency increased from -37.2dB to -23.1dB. In the second optimized design, the resonance frequency, dropped to 5.23GHz, and the refection coefficient was reduced to -35.7dB.

The performance of the antenna was obtained while the antenna was placed 1mm above the tissue layers with the surface area of 20x20mm^2. The performance of the antenna is summarized in Table 27. The gain of optimized antenna 1 slightly dropped, but insignificant increment was observed in the gain of optimized antenna 2.

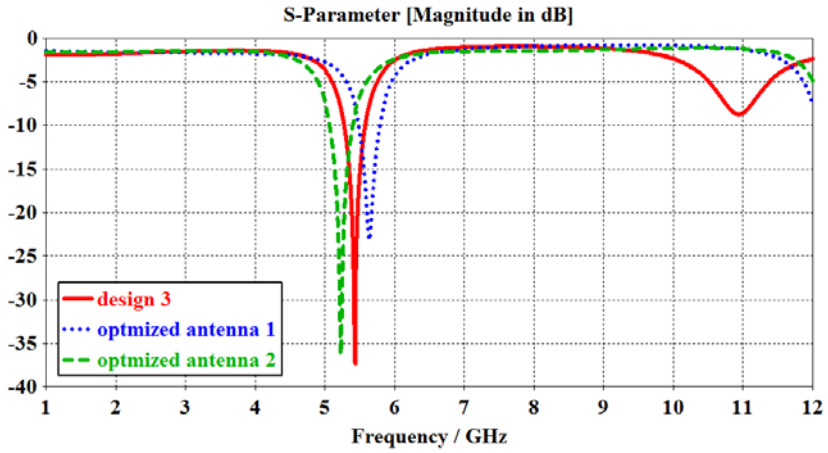

Figure 63. Reflection coefficient of modified antenna in section 3.5 (design 3), optimized antenna 1 and optimized antenna 2.

Table 27: Performance of antenna 3, optimized antenna.

Antenna	Frequency (GHz)	S_{11} (dB)	Gain (dBi)	Efficiency (%)	Directivity (dBi)
Design 3	5.43	-37.2	-7.95	8.34	2.84
Optimized 1	5.64	-23.1	-8.32	8.26	2.53
Optimized 2	5.23	-35.7	-6.84	9.71	3.29

5.4 Tissue Layers Curvature Study

A comparison of the optimized antenna 2 performance on square and curvy tissue layers was performed. The purpose of this study is to check if there is any change in antenna performance when the tissues surface is not planar, since in the real applications the body curvature might affect antenna performance. The shape and the dimensions of the tissues are shown in Figure 64. Figures 65-66 and Table 28 prove that the resonance frequency and the radiation pattern did not change with shape of the surface. However, the gain of antenna above curvy surface is less than the gain above planar one, and the directivity above curvy surface is less than the directivity above planar one.

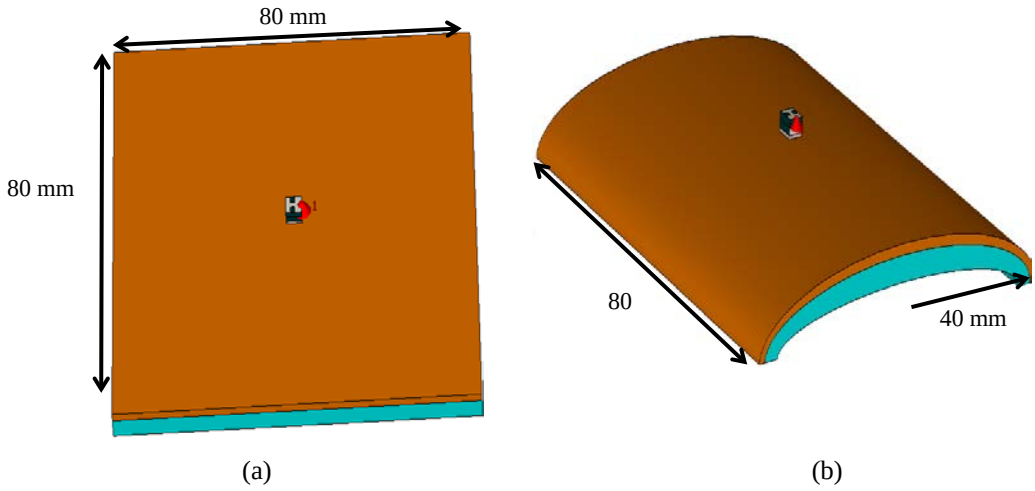

Figure 64. (a) Cubic tissue layers, and (b) curvy tissue layers.

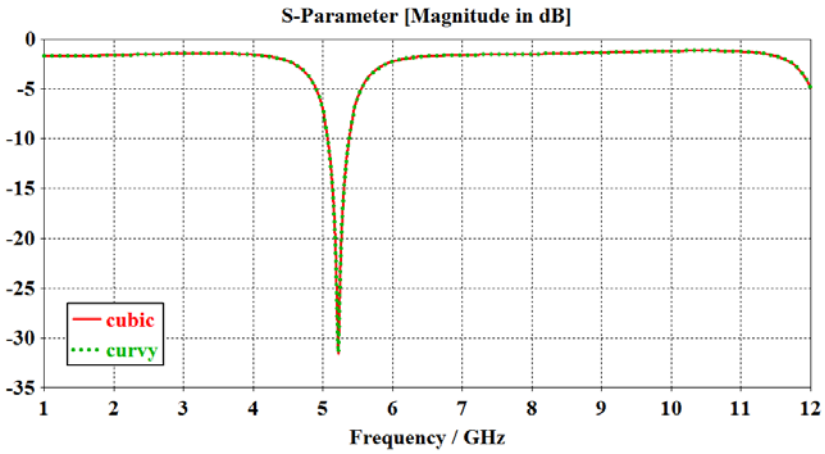

Figure 65. Reflection coefficient of antenna on cubic and curvy tissue layers.

Table 28: Antenna performance on cubic and curvy tissue layers.

Antenna	Gain (dBi)	Efficiency (%)	Directivity (dBi)
Cubic	-7.40	5.11	5.523
Curvy	-8.32	5.47	4.529

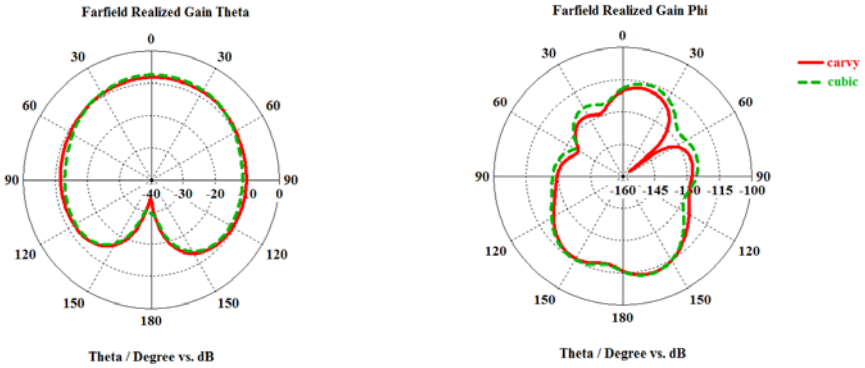

X-axis

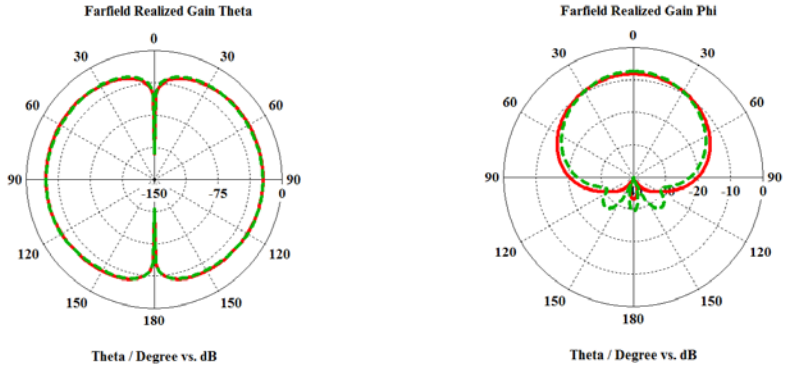

Y-axis

Figure 66. Radiation patterns of antenna on cubic and curvy tissue layers.

5.5 Experiment

5.5.1 Introduction

The antennas studied in the previous chapters and sections were only based on simulations. In this section, an antenna was fabricated and tested in free-space and on a phantom that mimics skin and fat layers. The purpose of this study was to observe the realistic performance of the miniaturized antenna and compare it to the simulated one. The fabricated antenna is connected to transmission cable. Hence, we wanted to perceive the effect of the transmission line on the antenna and the extent that it would be different from the simulation results as in simulations the feeding was done through a port and the line was not included in the simulations.

5.5.2 Phantom Experiment

Phantoms mimicking skin and fat tissues were made. The material selections and procedure for creating the phantoms were based on [42]. The materials and their weights and layer thicknesses are listed in Table 29.

Table 29: Materials for making the phantom[42].

layer	**thickness**	**Distilled water**	**Safflower oil**	**Propylene Glycol**	**Gelatin**	**Formalin**	**surfactant**
Skin	3 mm	80.00 g	14.00 g	7.00 g	5.88 g	0.30 g	0.30 g
Fat	7 mm	40.00 g	39.00 g	2.00 g	7.00 g	0.30 g	0.30 g

The procedure was simply mixing the distilled water with propylene glycol in a container while placed in a stove. The stove was at a temperature of 50^{o} C. When the mixture temperature reached 50^{o} C, the gelatin was added in the mixture and it was completely dissolved after mixing. At the same time of mixing the gelatin in the mixture

oil was mixed with surfactant and formalin. Then, everything was mixed together. Stirring the mixture was performed and the mixture was poured into cylindrical containers. Note that when we poured the fat phantom first in the container then the skin phantom, the skin phantom was dissolved into the fat phantom. Therefore, the skin phantom was poured into the container first and then the fat phantom was poured. Also, some of the containers were filled with skin phantom only, to be used for testing the antenna while it is implanted inside as discussed in the next section. Finally, the containers having the mixture were put in the refrigerator overnight. The phantoms are shown in Figure 67.

The dielectric properties of the phantom were obtained using Agilent 85070E Dielectric Probe, as shown in Figure 68. The temperatures of the layers were slightly lower than the room temperature. The first order Debye and measured dielectric properties of skin and fat phantoms at 3.017 GHz are listed in Table 30. Small pieces of phantom layers were obtained as seen in Figure 69.

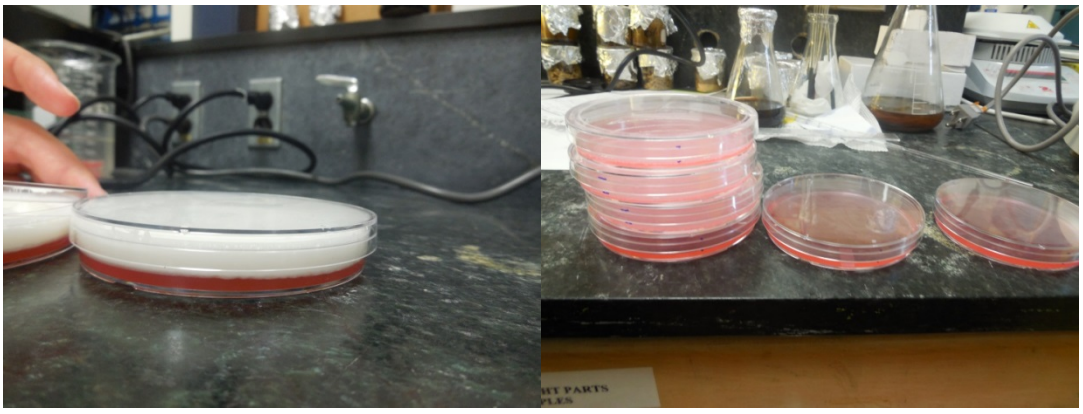

(a) (b)

Figure 67. (a) Skin and fat phantom layers, (b) skin phantom only.

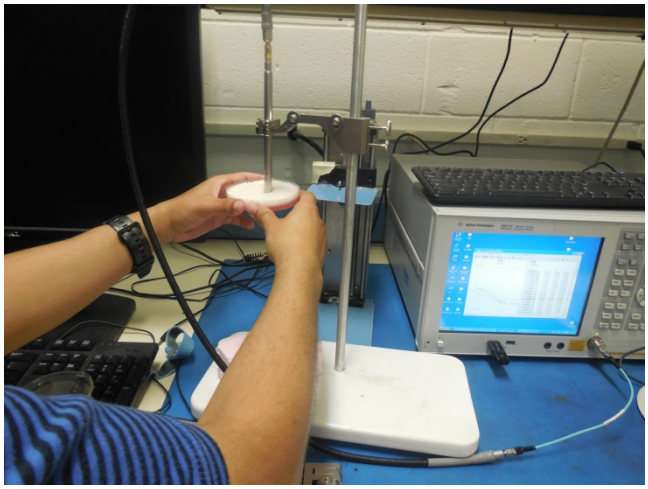

Figure 68. Dielectric properties measurment of phantom.

Figure 69. Different layers slices for testing.

Table 30: Measured and simulated dielectric properties of skin and fat.

Material	**Measurement 1**			**Measurement 2**			**Average**			**Debye Model curve in CST**		
	ε’	ε’’	σ	ε’	ε’’	σ	ε’	ε’’	σ	ε’	ε’’	σ
Skin	50.7	12.8	2.2	50.2	11.8	2.1	50.5	12.3	2.1	39	4.9	0.8
Fat	11.5	2.8	0.5	8.9	1.6	0.3	10.2	2.2	0.4	5.3	0.5	0.1

The dielectric properties of skin and fat phantoms in measurement are higher than dielectric properties of Debye model in CST. From literatures, it is known that water has high dielectric properties and is used to change the properties significantly. However, we believe this is not the reason since we used the same amount of ingredients. One possible reason is the difference in the temperature during making the process. In [42], a significant emphasis was put on temperature while mixture was being made. Another reason, as mentioned in [42], might be from the change in partial pressure which leads to gas removal and permittivity increase.

5.5.3 Antenna Structure

The antenna discussed in Section 3.1 was fabricated using MakerBot replicator 3D printer, as seen in Figure 70. Since the resolution of the device cannot reach the original dimensions of the antenna, the antenna was fabricated in larger size. Hence, the antenna structures in CST and after fabrication are depicted in Figures 71 and 72, and its new dimensions are given in Table 31.

Figure 70. MarkerBot replicator.

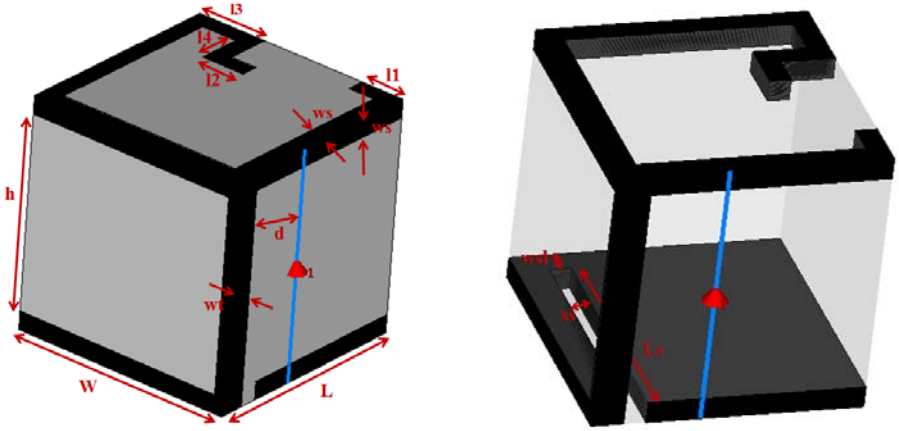

Figure 71. Fabricated antenna structure with dimensions in CST.

Table 31: Dimensions of fabricated antenna.

Parameters	Value (mm)	Parameters	Value (mm)
W	5.0	ws	0.4
L	5.0	l1	1.0
d	2.0	l2	1.0
h	4.2	l3	1.2
wt	0.6	l4	1.0
Ls	4.5	wsl	0.5
		ss	0.4

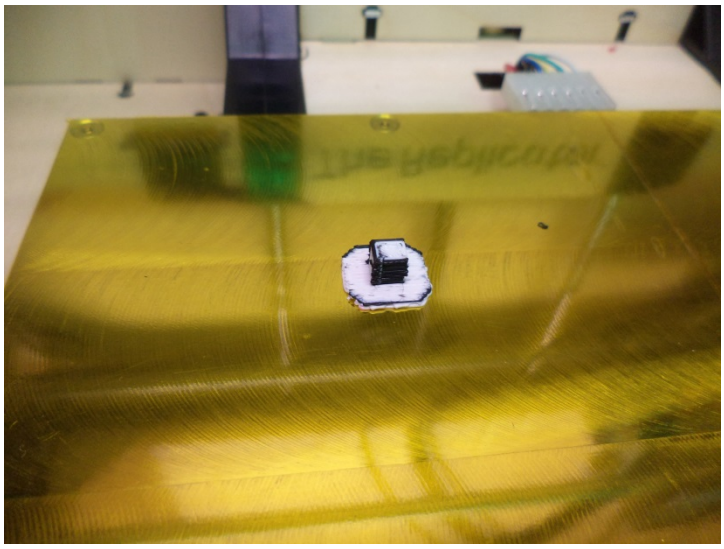

Figure 72. Antenna fabricated in MakerBot replicator.

The material used for substrate and conductive layers with dielectric properties at 6. 014 GHz are listed in Table 32. RG 316 coaxial cable was connected to the antenna with wire glue. The length of the cable is 13 cm. The fabricated antenna with transmission line is depicted in Figure 73.

Table 32: Dielectric Properties of materials used for fabricating the antenna.

Material	**Measurement 1**		**Measurement 2**		**Average**	
	ε’	ε’’	ε’	ε’’	ε’	ε″
ABS (White)	1.67	0.79	2.34	0.89	2.00	0.84
Conductive ABS (black)	10.47	5.06	10.39	5.47	10.43	5.26

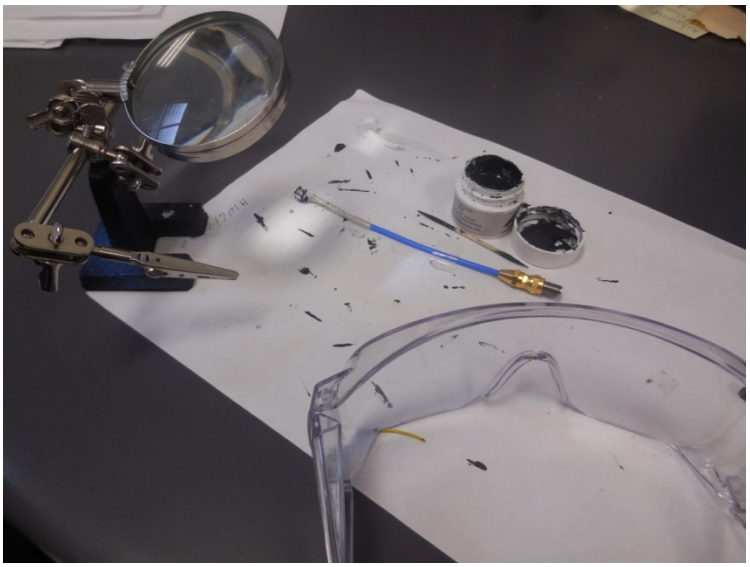

Figure 73. Antenna connected to a transmission line with wire glue.

5.5.4 Antenna-Phantom Experiment

Agilent E5071C ENA Network analyzer was used to obtain the resonance frequency of the antenna (Figure 74). Five major cases were done to see the antenna performance. These cases are free-space (case 1), on skin and fat phantom layers (case 2), on fat phantom only (case 3), sandwich between skin and fat phantoms layers (case 4), sandwich between fat phantom layers (case 5). The first two cases are for measurement and simulation comparison that were discussed in Chapter 3. Case 3 is to observe the effect of low dielectric tissue. Case 4 and case 5 were meant to measure the antenna resonance frequency and antenna performance while the antenna was embedded inside the body. Nevertheless, case 4 and case 5 are different. In case 4, the antenna was within fat and skin layers. In case 5, the antenna was put between two fat pantoms. The difference in the two cases is illustrated in Figure 75, and Figure 76 shows the realistic

five cases. The resonance frequencies of these five experiments are presented in Figure 77-81. Table 33 lists the bandwidth of the antenna in the five cases.

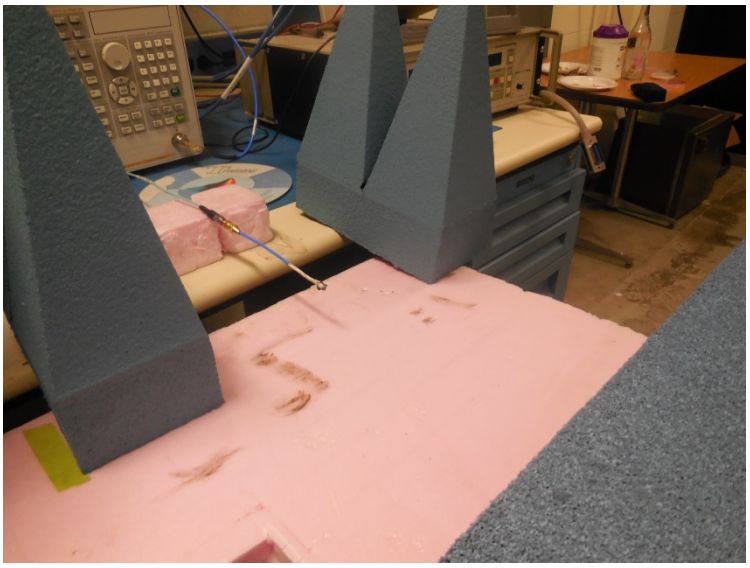

Figure 74. Antenna connected to E5071C network analyzer.

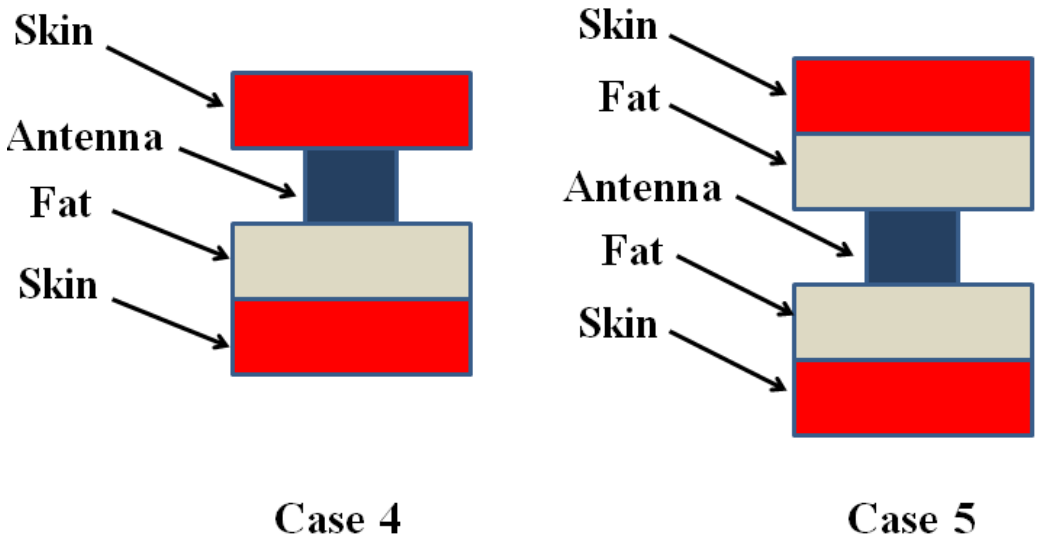

Figure 75. Layers arrangement showing the difference between case 4 and case 5.

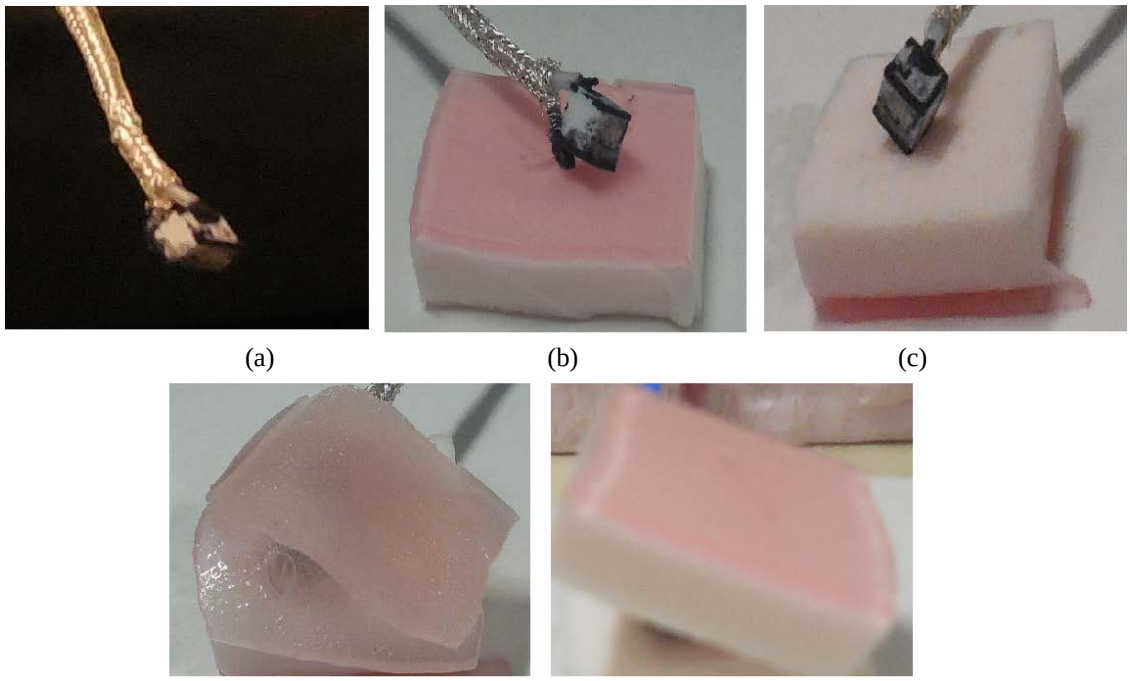

(a) (b) (c)

(d) (e)

Figure 76. Measurements in (a) case1, (b) case 2, (c) case 3, (d) case 4, (e) case 5, pink layer is sikn phantom, white layer is fat phantom.

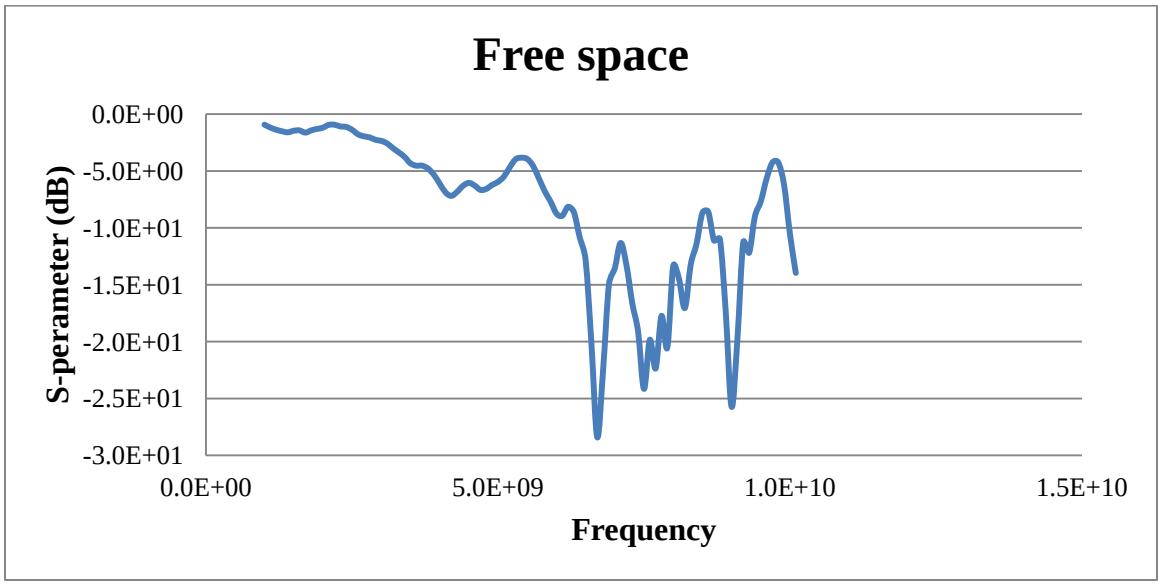

Figure 77. Measure reflection coefficient of antenna in free space.

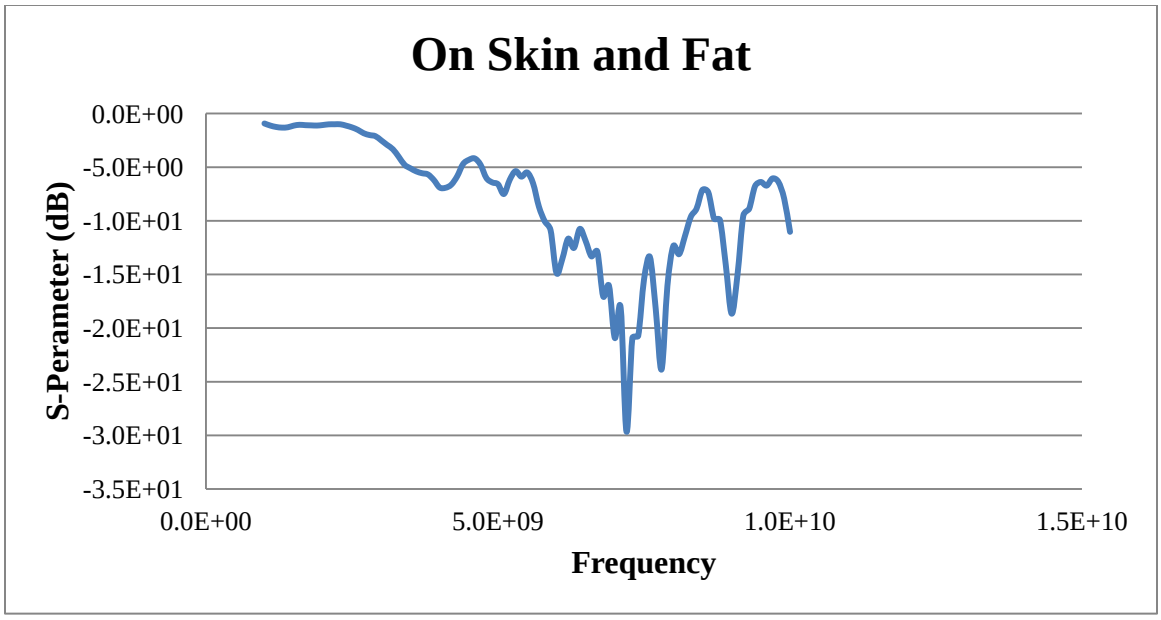

Figure 78. Measure reflection coefficient of antenna on skin and fat layers.

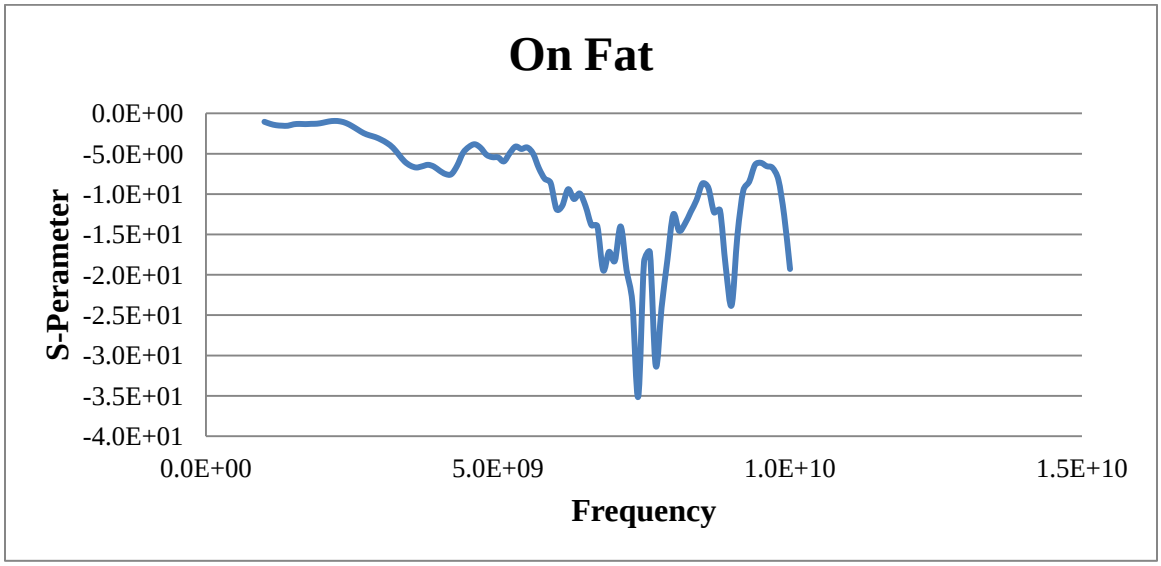

Figure 79. Measure reflection coefficient of antenna on fat.

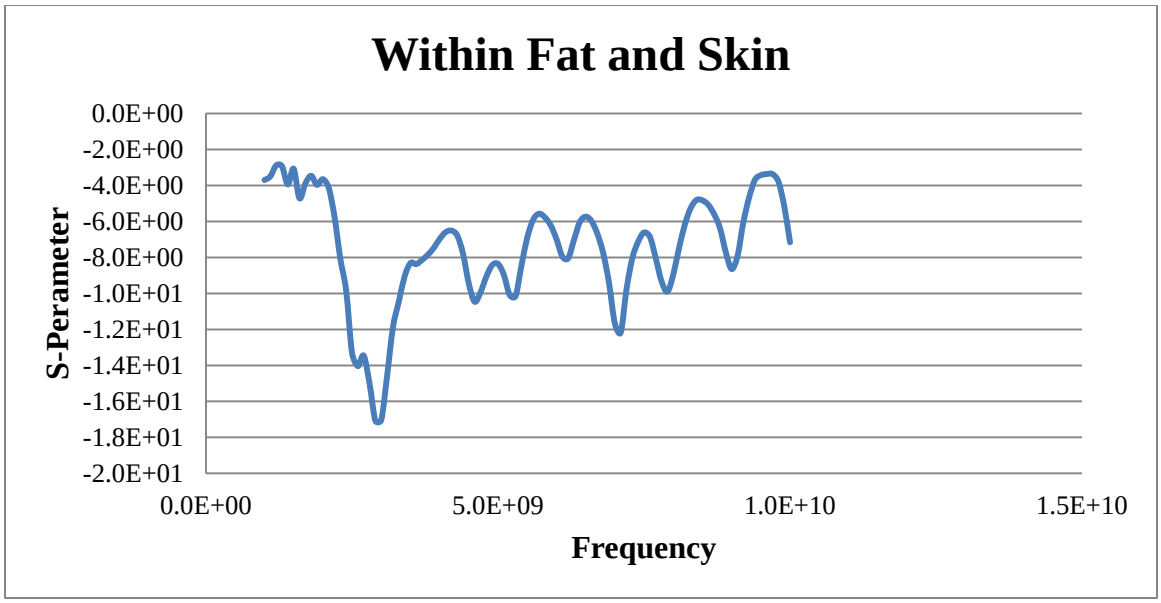

Figure 80. Measure reflection coefficient of antenna within fat and skin.

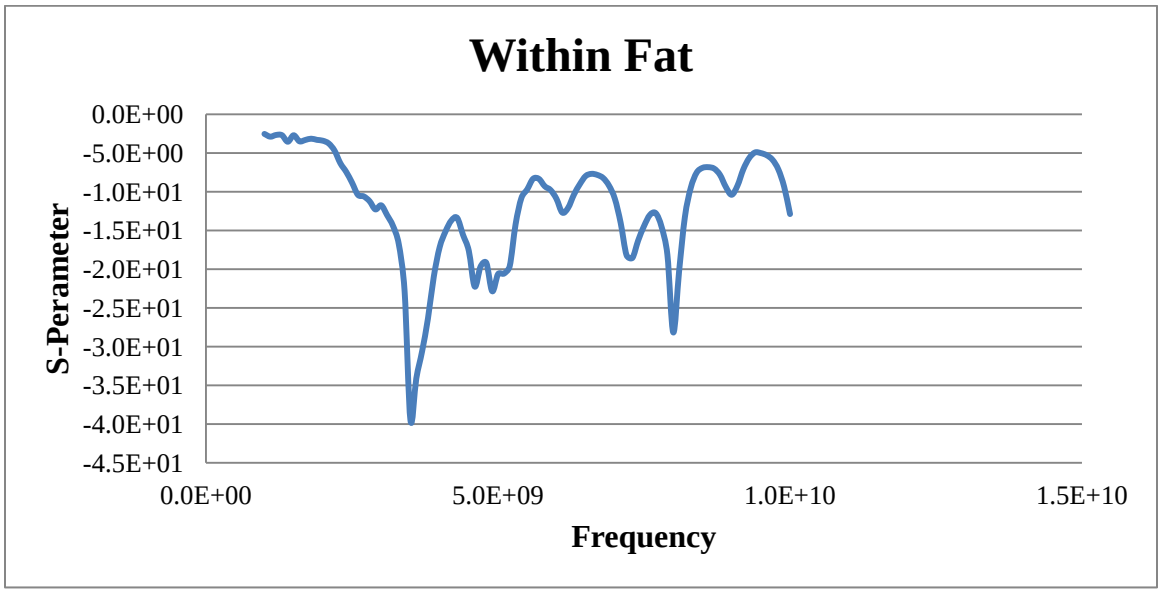

Figure 81. Measure reflection coefficient of antenna within fat.

Case1, case2, and case3 are almost the same as listed in Table 33. The presence of phantoms did not make changes in the resonance frequency. The reason might be the air gap between the ground of the antenna and the phantom layers that was made due to the

cable attached to the ground, as shown in Figure 82. In case 4 and case 5, there is a shift in resonance frequency to lower values, as explained in Chapter 4, resulted from the loading effect of the tissue layers. The permittivity of the layers slows down the waves. As a result, the electrical length increases and the resonance frequency decrease. In addition, it must be noted that the antenna was tested without being enclosed within a biocompatible material.

Table 33: Bandwidth of antenna in five cases.

Case	Name of the Case	Bandwidth
1	Free space	6.3 GHz- 9.3 GHz
2	On skin and fat	5.7 GHz-9.2 GHz
3	On fat	5.9 GHz- 9.2 GHz
4	Within fat and skin	2.4 GHz-3.4 GHz
5	Within fat	2.5 GHz- 5.5 GHz

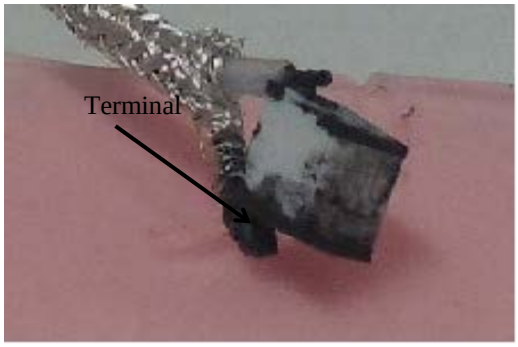

Figure 82. Node illustration.

The received power of the antenna was measured by Frequency generator and spectrum analyzer (Figure 83). The fabricated PIFA antenna was the receiver and a 2-18 GHz- horn antenna was the transmitter. The distance between the two antennas was 15 cm. the noise floor was -50 dBm. The results of this measurements are given in Table 34. The received power level ranges from -38 dBm to -33 dBm.

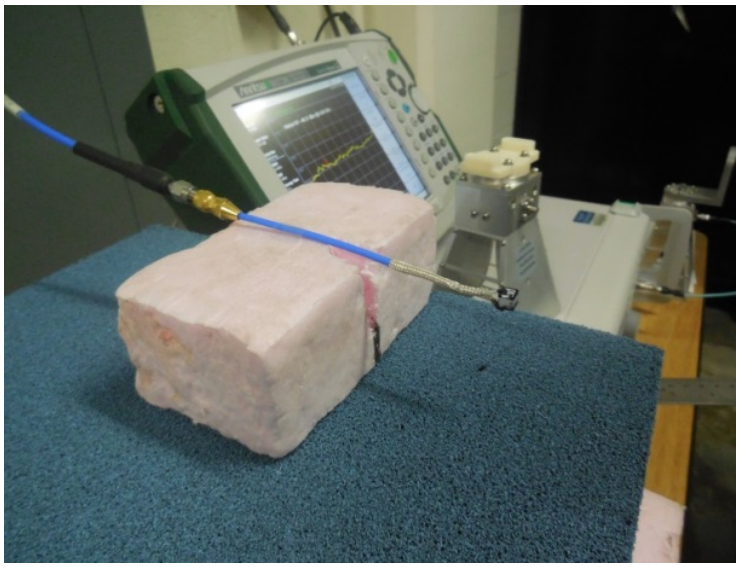

Figure 83. Antenna connected to spectrum analyzer.

Table 34: Radiation power of antenna in five cases with bandwidth and frequencies.

Case	**Name of the Case**	**Bandwidth**	**Power (dBm)**			
			3 (GHz)	**6 (GHz)**	**7 (GHz)**	**8 (GHz)**
1	Free space	6.3 GHz- 9.3 GHz	---	---	-35	-38
2	On skin and fat	5.7 GHz-9.2 GHz	---	-37	-35	-35
3	On fat	5.9 GHz- 9.2 GHz	---	-35	-33	-33
4	Within fat and skin	2.4 GHz-3.4 GHz	-30	---	---	---
5	Within fat	2.5 GHz- 5.5 GHz	-33	---	---	---

5.5.5 Experiments versus Simulation

The antenna with realistic size and materials (similar to the one that was fabricated) was simulated in CST with feeding as a port. The purpose was to observe the effect of the transmission line. Figure 84 shows that the antenna does not have resonance frequency within 1-10 GHz. It was concluded that a coaxial cable has a major effect on the fabricated antenna performance. Hence, a transmission line design should be considered in CST to create similar structure to the realistic one.

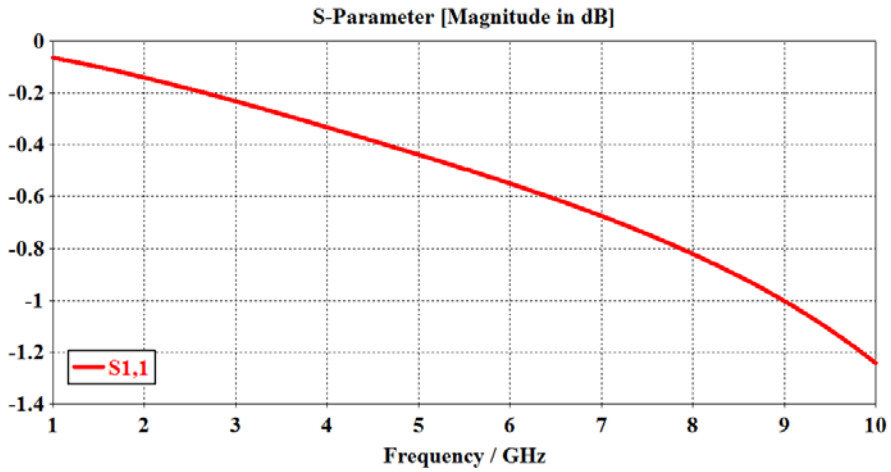

Figure 84. Reflection coefficient of antenna without transmission line in CST.

CHAPTER 6 FUTURE WORK

6.1 Introduction

In this thesis, several antennas with good performance were designed for wireless sensor applications. However, several issues should be considered in future studies.

First, the performance of simulated antenna was observed by using a port as source; in reality, a transmission line is used as a medium for transferring signal from the antenna to the receiver or from transmitter to the antenna. Due to the antenna size transmission line might have significant effects on radiation. These effects should be studied carefully and proper transmission line should be designed. Another issue is that a further study on a substrate with magnetic properties should be performed.

Most of the studies in this thesis are based on simulation. Antennas should be fabricated, tested and measurement results should be compared with simulated ones.

6.2 Transmission Line Design

One of miniature antenna applications is bio-compatible implanted sensors system. One application is to measure *in vivo* dielectric properties. The proposed idea is to implant a sensor inside a small animal, such as rats, and connect it to antenna that is placed outside the body via transmission line.

Transmission line is a medium for transferring signals in terms of voltage of current between a transceiver and the antenna. Some of transmission line types are

coaxial cable, strip line and microstrip line. Transmission line for sensor-antenna system will be narrow, small, and partly inside the rat's body, as depicted in Figure 85. Also, the transmission line should be placed in a shielding surface as it passed through organs inside the body. The reason is that the organs have high dielectric constant and conductivity, which may affect the performance of transmission lines.

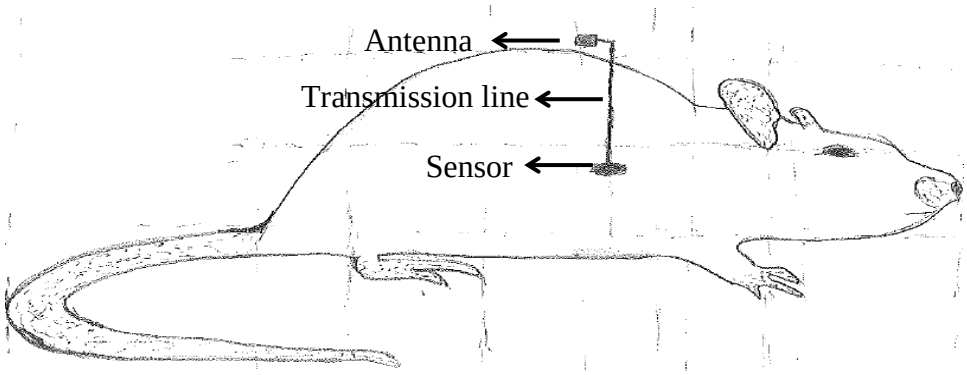

Figure 85. Sensor-antenna system in a rat.

6.3 Dielectric Magnetic Substrate

In the previous chapters, we used substrate with only one magnetic characteristic. Studying various magneto-dielectric substrates with different characteristics in CST Microwave Studio is necessary to study the influence of magnetic material on antenna performance. For example, in Table 22 in Chapter 5, the relative permeability is 2 and dielectric constant is 12. One step is to increase the relative permeability, keeping the dielectric constant as it is, or vice versa. The fabrication of desired magneto-dielectric layers with the desired characteristics is also a challenging task.

6.4 Fabrication Methods

The antenna should be fabricated and the results should be compared with the simulation results. Various methods for 3D printing are suggested: computer numerical control (CNC), stereo lithography (SLA), photolithography.

6.4.1 CNC

CNC machine is used for industrial applications. The operation is performed by numerical command that is set and stored in a computer. The commands are translated to electrical currents that move the motors of the machine to do specific task such as drilling, milling, contouring, gear boring, and reaming [43].

6.4.2 Stereo lithography

It is process of building 3D object by pointing ultraviolet laser beam to a photopolymer resin which is a liquid plastic. The idea of the process is based on the reaction between the light and the resin which causes the resin to become solid [44].

6.4.3 Photolithography

It is an etching process that is achieved by emitting ultraviolet light through photo mask onto a substrate. The substrate is coated with light sensitive chemical. When the light beam is focused on the substrate, a chemical reaction is performed on the exposed area making a route for electrical current transfer [45].

REFERENCES

[1] A. Rosen, M. A. Stuchly, and A. V. Vorst," Applications of rf/microwaves in medicine," *IEEE Transactions on Micorwave Theory and Techniques*, vol. 50, no. 3, pp. 963-974, March 2002.

[2] N. Chahat, M. Zhadobov, R. Saulaeau, and K. Ito, "A compact UWB antenna for on-body applications," *IEEE Transactions on Antennas Propagation.*, vol. 59, pp. 1123-1131, April 2011.

[3] R. Warty, M. Tofighi, U. Kawoos, and A. Rosen, "Characterization of implantable antennas for intracranial pressure monitoring: reflection by and transmission through a scalp phantom," *IEEE Transactions on Microwave Theory and Techniques,* vol. 56, no. 10, pp. 2366-2376, Oct. 2008.

[4] S. M. Islam, K. P. Esselle, D. Bull , and P. M. Pilowsky, "Design of an implantable antenna to acquire physiological signals in rats," *IEEE Transactionsons on Antennas Propagation,* July 2012.

[5] K. Fujimoto, A. Henderson, K. Hirasawa, and J. James, *Small Antenna*. Letch worth, Herts: RESEARCH STUDIES PRESS LTD, 1987.

[6] J. Abadia, F. Merli, J-F Zurcher, J. R. Mosig, and A. K. Skrivervik, " 3D-spiral small antenna desing and realization for biomdeical telemetry in the MICS band," *Radioengineering,*vol. 18, no. 4, pp. 259-367, Dec 2009.

[7] T. Dissanayake, K. P. Esselle, and M. R. Yuce, " Dielectric loaded impedance matching for wideband implanted antennas," *IEEE Transactions on Micorwave Theory and Techniques* , vol. 57, no. 10, pp. 2480-1562487, Oct. 2009.

[8] M. Lanciault, and J-D Richerd, "Examine antenna tunability in implanted system," Microwaves & RF, vol. 48, no. 12, pp74-78, Dec. 2009.

[9] M. Sadiku, *element of electromagnetics*, 3rd ed. New York: Oxford University Press, 2001.

[10] M. A. Stuchly, T-W Athey, S.S. Stuchly, G. M. Samaras, and G. Taylor, " Dielectric properites of animal tissue *in-vivo* at frequencies 10 MHz- 1 GHz," *Bioelectromagnetics*, vol. 2, pp. 93-103, 1981.

[11] J. Cho, J Yoon, S Cho, K Kwon, S Lim, D Kim, E S Lee, C Hwan K, J Wook C, C Cheon, and Y Kwon, "In-vivo measurements of the dielectric properties of breast carcinoma xenografted on nude mice," *Internation Journal of Cancer*, pp. 593-598, 2006.

[12] A P O'Rourke, M Lazebnik, J M Betram, M C Converse, S C Hagness, J G Webster, and D M Mahvi, "Dielectric properties of human normal, malignant and cirrhotic liver tissues: in vivo and ex vivo measurements from.5 to 20 GHz using a precision open-ended coaxial probe," *Pysics in Medicine and Biology*, pp. 4707-4719, 2007.

[13] A. Vorst, A. Rosen, and Y. Kotsuka, *RF / Microwave Interaction with Biological Tissues*. Hoboken, NJ: John Wiley & Sons, 2006.

[14] R. Pething, *Dielectric and electrical Properties of Biological Materials*. : John Wiley & Sons, 1979.

[15] R. Pethig and D. Kell. (1987. Feb.). "The passive electrical properties of biological systems: their significance in physiology, biophysics and biotechnology." *Phys. Med. Biol.*[On-line].

[16] N. Nikolova, "Microwave Imaging for Breast Cancer," *IEEE Microwave Magazine*, Vol. 12, pp. 78-94, Dec 2011.

[17] V. Komarov, S. Wang, and J. Tang. (2005). "Permittivity and Measurement." *Encyclopedia of RF and Microwave Engineering.* [On-line]. 4(308), pp. 1-21. Available: http://www.bsyse.wsu.edu/ifafs/paper/dp-rf-mw.pdf [March 28, 2013].

[18] C. Gabriel, S Gabriel, and E Corthout, "The Dielectric properties of biological tissues: III. parametric models for the dielectric spectrum pf tissues," *Physics in Medicine and Biology*, pp. 2271-2293, 1996.

[19] K. Barrese, and N. Chugh, "Approximating dispersive mechansims using the Debye model with distributed dielectric parameters,".

[20] Agilent, *Basics of Measuring the Dielectric Properties of Material*, Available http://www3.imperial.ac.uk/pls/portallive/docs/1/11949698.PDF visited Feb. 2013.

[21] G. Mazarei, "In vivo, in vitro, ex vivo," Internet: http://www.askmedicalresearchers.com/in-vivo-in-vitro-ex-vivo/, Nov. 9, 2014[July 2014].

[22] R. J. Halter, T. Zhou, P.M. Meaney, A. Hartov, R.J. Barth Jr, K.M. Rosenkranz, W.A. Wells, C.A. Kogel, A. Borsic, E.J. Rizzo and K.D. Paulsen, "The correlation of *in vivo* and *ex vivo* tissue dielectric properties to validate electromagnetic breast imaging: initial clinical experience," *Physiological Measurement*, vol. 30, pp. 121-136, June 2009.

[23] A. Kraszewski, M. A. Stuchly, S. S. Stuchly, and andrew M. Smith," *In-vivo* and i*n-vitro* dielectric properites of animal tissues at radio frequencies," *Bioelectromagnetics,* vol. 3, pp. 421-432, 1982.

[24] A. M. Campbell, and D. V. Land," Dielectric properties of female human breast tissue measured *in vitro* at 3.2 GHz," *Physics in Medicine and Biology*, vol. 37, no. 1, pp. 193-210, June 1991.

[25] A. Swarup, S. S. Stuchly, and A. Surowiec, "Dielectric properties of mouse MCA1 fibrosarcoma at different stages of development," *Bioelectromagnetics,* vol. 12, pp. 1-8, 1991.

[26] T. H. Kim, and J. K. Pack, " Measurment of electrical characteristics of female breast tissues for the development of the breast cancer detector," *Progress in Electromagnetics Research C,* vol. 30, pp. 189-199, 2012.

[27] J. L. Volakis, *Antenna Engineering Handbook*. New York, 4th ed. NY: Mc Graw-Hill, 2007.

[28] C. A. Balanis, *Antenna Theory: Analysis and Design,* 2nd ed. New York: Wiley, 2005.

[29] C. A. Balanis, *Modern Antenna Handbook,* Hoboken, NJ: Wiley,2008.

[30] R. Kastner. "Limitations on small antennas-implications to RF engineering." Internet: http://www.youtube.com/watch?v=BZ0OTNFlTg0 , Jan. 8, 2014[May 11, 2013.

[31] Y. Thierry and J. Charles," Effects of Substrate Permittivity on Planar Inverted-F Antenna Performances," *JOURNAL OF COMPUTERS*, Vol. 4, pp. 610- 614, July 2009.

[32] J. L. Volakis, C. Chen, and K. Fujimoto, *Small Antennas*. New York, NY: McGraw-Hill, 2010, pp. 188-199..

[33] CST Microwave Studio, www.cst.com, visited December 2013.

[34] A. Sabouni and S. Noghanian, "Study of penetration depth and noise in microwave tomography technique," *Applied Computational Electromagnetics Society Journal*, vol. 28, pp. 391, May 2013.

[35] Y-X. Guo, M.Y.W. Chia, and Z. N. Chen, "Miniature built-in quad-band antennas for mobile handsets," *IEEE Antennas and Wireless Propagation Letters*, vol. 2, pp. 30-32, 2003.

[36] Rogers Corporation, "*RT/duroid® 5870 /5880 high frequency laminates*," [Online], Available: http://www.rogerscorp.com/documents/606/acm/RT-duroid-5870-5880-

Data-Sheet.aspx [July 30, 2014].

[37] L. P. Yan, K. M. Huang, and C. J. Lui, “A noninvasive method for determining dielectric properties of layered tissues on human back,” *J. of Electromagn. Waves and Appl.*, vol. 21, pp. 1829-1843, 2007.

[38] A. Cabedo, J. Anguera, C. Picher, M. Ribo, and C. Puente, “Multiband handset antenna combining a PIFA, slots, and ground plane modes,” *IEEE Trans. Antennas Propag.*, vol. 57, pp. 2526-2533, September 2009..

[39] M. A. Eleiwa, A. Z. Elsherbeni, “Debye constants for biological tissues from 30 Hz to 20 GHz,” *ACES Journal*, vol. 16, no. 3, pp. 202-213, 2001.

[40] http://niremf.ifac.cnr.it/tissprop/ , visited March 2014.

[41] M. Aldrigo, A. Costanzo, D. Masotti, and C. Galassi," Exploitation of a novel magneto-dilectric substrate for miniaturization of wearable UHF antennas," *Materials Letters*, vol. 87, pp. 127-130, 2012.

[42] C. Hahn, and S. Noghanian," Heterogeneous breast phantom development for micowave imaging using regression models," *Hindawi International Journal of Biomedical Imaging.* vol. 2012, pp. 1-12, 2012.

[43] S. Krar, A. Gill, and P. Smid. *Computer Numerical Control.* New York, NY: Industrial Press Inc, 2001.

[44] "How stereolithography (SLA) works." Internet:https://thre3d.com/how-it-works/light-photopolymerization/stereolithography-sla, [July 2014].

[45] "What is photolithography?" Internet:http://www.tech-faq.com/photolithography.html, May 13, 2014[July 2014].